A TOKAMAK EXPERIMENTAL POWER REACTOR

REACTORS

KEYWORDS: *Tokamak devices, power plants, design, engineering, first wall, breeding blankets, neutral atom beam injection, plasma confinement, size*

W. M. STACEY, Jr., V. A. MARONI, J. R. PURCELL, M. A. ABDOU, P. J. BERTONCINI, J. N. BROOKS, J. B. DARBY, Jr., K. EVANS, Jr., J. A. FASOLO, R. L. KUSTOM, J. S. MOENICH, J. S. PATTEN, D. L. SMITH, H. C. STEVENS, and S. T. WANG *Argonne National Laboratory, CTR Program, 9700 South Cass Avenue, Argonne, Illinois 60439*

Received August 4, 1975
Accepted for Publication February 23, 1976

The Division of Controlled Thermonuclear Research/U.S. Energy Research and Development Administration Program Plan for the development of Tokamak power reactors calls for a first Tokamak experimental power reactor (TEPR) to begin operation in 1985 to 1987. For the past year, an interdisciplinary project at Argonne National Laboratory (ANL) has been engaged in scoping and project definition studies for the TEPR. A preliminary conceptual design was developed to provided a focus for the studies. The ANL-TEPR has a major radius, $R = 6.25$, and a plasma radius, $a = 2.1$ m. Sixteen, pure-tension-D superconducting magnets, with minor bore, $R_{bore} = 7.7$ m, and vertical bore, $Z = 11.9$ m, provide a toroidal field of 34 kG in the plasma, with a maximum field ripple of 2%. A stainless-steel–B_4C blanket/shield, which is 1 m on the inside and 1.3 m on the outside, protects the magnets and converts the nuclear energy to sensible heat, which is removed by the primary coolant, helium or H_2O. The first wall is 2-cm-thick stainless steel with a 100-μm low-Z coating on the plasma side, and operates at ≤550°C. The toroidal vacuum chamber is pumped down from 10^{-3} to 10^{-5} Torr between burn pulses by thirty-two 25 000 ℓ/s cryosorption pumps, and 50 000 ℓ/s cryosorption panels maintain the vacuum in the neutral beam injectors, which are used to heat the plasma.

Burn pulses of 20 to 60 s, interrupted by a 15-s exhaust and replenishment phase, are envisioned for the TEPR. The plasma properties at equilibrium are [$n\tau = 0.56 \times 10^{20}$ m^{-3}, $T = 10$ keV, $\beta_\theta = 2.2$, $q = 2.5$, $I_p = 4.8$ MA, $P_T = 129$ MW(th)]. Plasma heating is accomplished by 40 MW of 180-keV neutral deuteron beam for 3 s. Approximately 100 V-s are required to induce the plasma current and maintain it against resistive losses, which requires a plasma driving system power supply that can deliver ~450 MJ, with a peak power demand of ~1000 MW(e). The V-s are provided by superconducting ohmic-heating ($\frac{2}{3}$) and equilibrium ($\frac{1}{3}$) field coils located external to the toroidal field coils. Approximately 30-MW(e) cycle-average power ($\eta = 0.3$) can be produced. If confinement is adequate for ignition ($n\tau = 4.2 \times 10^{20}$ $s/m^3 = 10 \times$ TIM), the net electrical power, after subtracting the power required to produce the neutral beam ($\eta = 0.5$) and the nonrecovered energy provided by the plasma driving system ($\eta = 0.95$), is 15 to 20 MW(e). If confinement is as poor as predicted by trapped-ion-mode (TIM) theory, 23 MW of supplemental neutral-beam heating are required to maintain the power balance, and the net electrical power is negative, although the 30-MW(e) power level can still be attained. Approximately 16 g of tritium would be consumed for each full-power day of operation.

Cryogenically stable superconducting toroidal field (TF), ohmic-heating (OH), and equilibrium field (EF) coils are proposed for the TEPR. The superconductor is NbTi, with a copper (plus cupronickel for the OH and EF coils) stabilizer and stainless steel. The average current densities are 1280 A/cm^2 in the TF and OH coils and 2300 A/cm^2 in the EF coils. The peak fields are 75 kG in the TF coils, 37 kG in the EF coils, and 32 kG in the OH coils. The maximum hoop-stress level in the support system for the TF coils is ~24 000 psi.

A stainless-steel first wall is expected to maintain its structural integrity for integrated neutron wall loadings in excess of 1 MW-yr/m^2, which would permit over ten years of operation at 0.2 MW/m^2 with a 50% duty factor. The blanket/shield was designed to allow the same operation

M. Abdou - 208

A TOKAMAK EXPERIMENTAL POWER REACTOR

REACTORS

KEYWORDS: *Tokamak devices, power plants, design, engineering, first wall, breeding blankets, neutral atom beam injection, plasma confinement, size*

W. M. STACEY, Jr., V. A. MARONI, J. R. PURCELL, M. A. ABDOU, P. J. BERTONCINI, J. N. BROOKS, J. B. DARBY, Jr., K. EVANS, Jr., J. A. FASOLO, R. L. KUSTOM, J. S. MOENICH, J. S. PATTEN, D. L. SMITH, H. C. STEVENS, and S. T. WANG *Argonne National Laboratory, CTR Program, 9700 South Cass Avenue, Argonne, Illinois 60439*

Received August 4, 1975
Accepted for Publication February 23, 1976

The Division of Controlled Thermonuclear Research/U.S. Energy Research and Development Administration Program Plan for the development of Tokamak power reactors calls for a first Tokamak experimental power reactor (TEPR) to begin operation in 1985 to 1987. For the past year, an interdisciplinary project at Argonne National Laboratory (ANL) has been engaged in scoping and project definition studies for the TEPR. A preliminary conceptual design was developed to provided a focus for the studies. The ANL-TEPR has a major radius, $R = 6.25$, and a plasma radius, $a = 2.1$ m. Sixteen, pure-tension-D superconducting magnets, with minor bore, $R_{bore} = 7.7$ m, and vertical bore, $Z = 11.9$ m, provide a toroidal field of 34 kG in the plasma, with a maximum field ripple of 2%. A stainless-steel–B_4C blanket/shield, which is 1 m on the inside and 1.3 m on the outside, protects the magnets and converts the nuclear energy to sensible heat, which is removed by the primary coolant, helium or H_2O. The first wall is 2-cm-thick stainless steel with a 100-μm low-Z coating on the plasma side, and operates at ≤550°C. The toroidal vacuum chamber is pumped down from 10^{-3} to 10^{-5} Torr between burn pulses by thirty-two 25 000 ℓ/s cryosorption pumps, and 50 000 ℓ/s cryosorption panels maintain the vacuum in the neutral beam injectors, which are used to heat the plasma.

Burn pulses of 20 to 60 s, interrupted by a 15-s exhaust and replenishment phase, are envisioned for the TEPR. The plasma properties at equilibrium are [$n\tau = 0.56 \times 10^{20}$ m^{-3}, $T = 10$ keV, $\beta_6 = 2.2$, $q = 2.5$, $I_p = 4.8$ MA, $P_T = 129$ MW(th)]. Plasma heating is accomplished by 40 MW of 180-keV neutral deuteron beam for 3 s. Approximately 100 V-s are required to induce the plasma current and maintain it against resistive losses, which requires a plasma driving system power supply that can deliver ~450 MJ, with a peak power demand of ~1000 MW(e). The V-s are provided by superconducting ohmic-heating ($\frac{2}{3}$) and equilibrium ($\frac{1}{3}$) field coils located external to the toroidal field coils. Approximately 30-MW(e) cycle-average power ($\eta = 0.3$) can be produced. If confinement is adequate for ignition ($n\tau = 4.2 \times 10^{20}$ $s/m^3 = 10 \times$ TIM), the net electrical power, after subtracting the power required to produce the neutral beam ($\eta = 0.5$) and the nonrecovered energy provided by the plasma driving system ($\eta = 0.95$), is 15 to 20 MW(e). If confinement is as poor as predicted by trapped-ion-mode (TIM) theory, 23 MW of supplemental neutral-beam heating are required to maintain the power balance, and the net electrical power is negative, although the 30-MW(e) power level can still be attained. Approximately 16 g of tritium would be consumed for each full-power day of operation.

Cryogenically stable superconducting toroidal field (TF), ohmic-heating (OH), and equilibrium field (EF) coils are proposed for the TEPR. The superconductor is NbTi, with a copper (plus cupronickel for the OH and EF coils) stabilizer and stainless steel. The average current densities are 1280 A/cm^2 in the TF and OH coils and 2300 A/cm^2 in the EF coils. The peak fields are 75 kG in the TF coils, 37 kG in the EF coils, and 32 kG in the OH coils. The maximum hoop-stress level in the support system for the TF coils is ~24 000 psi.

A stainless-steel first wall is expected to maintain its structural integrity for integrated neutron wall loadings in excess of 1 MW-yr/m^2, which would permit over ten years of operation at 0.2 MW/m^2 with a 50% duty factor. The blanket/shield was designed to allow the same operation

before the radiation-induced increase in resistivity of the TF stabilizer exceeded 2.5 × 10^{-8} Ω-cm, with a safety factor of 10. The nuclear heating in the TF coils causes a temperature rise of <0.05 K.

I. INTRODUCTION

The U.S. Energy Research and Development Administration (ERDA) Division of Controlled Thermonuclear Research (DCTR) Program Plan for the development of Tokamak power reactors[1] calls for a Tokamak fusion test reactor (TFTR) to begin operation in about 1980, a first Tokamak experimental power reactor (TEPR) to begin operation in 1985 to 1987, possibly a second TEPR to begin operation in about 1990, and a Tokamak demonstration power reactor (TDPR) to begin operation in 1995 to 2000. An interdisciplinary project at Argonne National Laboratory (ANL) is engaged in a conceptual design study for the first TEPR. The first stage of that study, a project definition study resulting in a preliminary conceptual design, has been completed.[2] This paper summarizes that study and provides insight as to the features of a TEPR and the required technology development.

II. TEPR OBJECTIVES

A major purpose of this study is to focus and refine the objectives for a TEPR by defining a scientifically and technologically feasible device that satisfies the programmatic requirements of the U.S. Tokamak Fusion Power Reactor Development Program. Such a device should represent the logical next step beyond the TFTR (Ref. 3) in the achievement of deuterium-tritium (D-T) plasma confinement adequate for power reactors. The TEPR should be a major step in the demonstration of engineering feasibility of Tokamak power reactors. It should provide experience with and demonstrate the feasibility of the various technologies involved and their synthesis in a power reactor environment, thereby serving as a focal point for the technology development program. It should also demonstrate the feasibility of electrical power production from fusion on a significant scale [in the range of 5 to 50 MW(e)], and, if possible, demonstrate the feasibility of electrical power breakeven. The TEPR should serve as a major test facility for the technology development program. These general objectives must be reconciled among themselves, with the state-of-the-art and required developmental programs for the various technologies, with the DCTR programmatic requirements for initial operation in 1985 to 1987, and with a yet unspecified fiscal constraint to arrive at a realistic set of specific objectives for a TEPR.

It is useful to divide the potential TEPR objectives into four categories:

1. Plasma Physics
   a. Heat, confine, and refuel a reactor-grade D-T plasma under such conditions that the production of 5 to 50 MW(e) of electrical power is feasible.
   b. Study plasma confinement, stability, heating, fueling, and control in the reactor regime.
2. Power Reactor Engineering Feasibility
   a. Remove sensible heat from an energy conversion blanket operating under high-temperature conditions such that generation of 5 to 50 MW(e) of electrical power is feasible.
   b. Demonstrate the feasibility of electrical power breakeven.
   c. Breed, extract, process, and recycle tritium under conditions such that a tritium breeding ratio greater than unity is demonstrable.
3. Technology Demonstration
   a. Superconducting magnets
   b. Plasma heating and fueling
   c. Vacuum systems
   d. Power supply and energy storage
   e. Primary coolant
   f. Tritium extraction, processing, and containment
   g. Materials
   h. Assembly, fabrication, and remote maintenance.
4. Test Facility Utilization
   a. Surface and bulk materials irradiation
   b. Blanket modules with different blanket design, materials, coolant, and tritium extraction concepts
   c. Other—components testing, plasma and reactor instrumentation, and control, etc.

The TEPR should be the logical next step beyond the TFTR (initial operation 1980) along the path to achievement of plasma confinement that is

adequate for a power reactor. Achievement of sufficient pulse length and pulse repetition rate so that the cycle-average thermonuclear power, if converted to electrical power, would be in the range of 5 to 50 MW(e), is a major goal for the TEPR. Conversion of this energy into sensible heat in an energy-conversion blanket is a second major goal. If these two goals could be achieved, conversion of the thermal energy in the primary coolant into electrical energy in a secondary system could be accomplished straightforwardly. These two objectives are sufficiently important in themselves that there is a strong motivation to minimize any other factors that might complicate or compromise their attainment. This consideration argues for a "minimum-risk" approach that utilizes, to the maximum extent possible, technology that is either state-of-the-art or extrapolated from it with reasonable confidence.

The minimum-risk approach is contrary to many of the general objectives envisioned for the TEPR. The specific technological choices (e.g., materials) might not be extrapolatable to a commercial power reactor, or at best, might not represent optimal choices for the latter. Certain functions of a commercial reactor (e.g., tritium breeding) are not essential to the plasma and sensible heat production objectives for the TEPR; such "extraneous" complications would certainly be eliminated in a minimum-risk design. A minimum-risk design does not provide a focus for a broad-base reactor technology development program, nor does it lead to a demonstration that the technology can be sufficiently developed so that a full-scale fusion power reactor is technologically feasible. Thus, there are strong arguments against the minimum-risk, or minimum technology development, approach and in favor of utilizing the TEPR as a vehicle for advancing the technologies that will be needed for fusion power reactors.

Staged operation is proposed as one means of reconciling these seemingly conflicting requirements. A minimum-risk approach would be followed in designing a device to achieve the plasma physics objectives, with an energy conversion blanket (no tritium breeding) to achieve the sensible heat-power objectives. The device would be operated during Stage I (approximately 1986 to 1989) to obtain these objectives and, in addition, to serve as a materials irradiation facility. Provision would be made in the design to replace one or more of the original blanket modules with alternate blanket test modules. During Stage II (approximately 1990 to 1995), the device would function primarily as a blanket test facility in which various blanket, tritium breeding and extraction materials and coolant concepts were studied under reactor conditions. Staged operation has a number of advantages:

1. The fundamental plasma-power objectives can be focused on first, with a minimum amount of complication.

2. Decisions to allocate funds for the blanket test modules can, to some extent, be made after the plasma physics objectives have been demonstrated.

3. Additional time is allowed for the development of the technologies required for a tritium breeding blanket, without delaying the overall TEPR schedule.

The disadvantages of staged operation are associated with the added complications to the basic design and to the remote breakdown and reassembly requirements.

The TEPR will represent a unique test facility. Its utilization as such should be factored into, but should not compromise, the basic design objectives.

Plasma confinement scaling and the effect of impurities are two major uncertainties that must be allowed for in the design. [Results from PLT (initial operation 1976) on confinement scaling and from Doublet-III (initial operation 1978) on plasma shape optimization, as well as results from PDX and ISX (initial operation 1977) on impurity control, will be available before the final design of the TEPR is fixed.] Allowance is made in the design for the attainment of many of the objectives even if the confinement scaling and impurity effects are less favorable than anticipated.

Demonstration of the feasibility of electrical power breakeven would be a dramatic achievement for the TEPR. Allowance for attaining this objective in the event of relatively unfavorable transport scaling and impurity effects would require substantial and expensive additional margin in the design relative to what would suffice to assure many of the other objectives. (This problem would be mitigated somewhat if Doublet-III and PDX demonstrate the anticipated advantages of noncircular cross-section plasmas.) However, a convincing demonstration of electrical power breakeven might well require the advance of certain technologies beyond the point that is compatible with the schedule, financial constraints, and general objectives of the TEPR. Thus, the decision to demonstrate electrical power breakeven feasibility should be deferred until the consequences are examined in detail and additional information is available from the plasma confinement experiments that will be conducted in the next few years.

The size of the TEPR, and hence its cost and

degree of extrapolation beyond preceding devices, scales with the power level, as will be discussed in Sec. III. This consideration argues for choosing a modest power level objective that will suffice for the demonstration of power reactor technology and will satisfy the criterion of "significant" power production. An electrical power output on the order of tens of megawatts is adequate for this purpose. On the other hand, electrical power breakeven becomes more plausible at larger power outputs, perhaps on the order of a hundred megawatts electrical. Achievement of 5- to 50-MW(e) power output, with provision for operation at higher levels if present plasma physics uncertainties turn out favorably, seems to be a reasonable objective.

A tentative set of TEPR objectives are summarized in Table I. These objectives will be periodically reviewed during the course of the conceptual design. As more comprehensive analyses are performed and the resulting requirements are compared with technology as it exists and as it can reasonably be expected to advance, the objectives and schedules of the TEPR and of the supportive technology development programs can be refined to best satisfy the overall programmatic objectives of the DCTR Tokamak Power Reactor Development Program.

III. FACTORS DETERMINING THE SIZE OF A TEPR

Three types of considerations guide the determination of size. The TEPR must be a justifiable and logical next step beyond the TFTR in Tokamak plasma confinement devices. On the other hand, it must be large enough to accomplish the power objectives of the TEPR. Finally, the cost constraint will impose a size limitation of a different type.

Table II provides some perspective on the evolution of Tokamak plasma confinement devices. Also shown in this table are the parameters for two conceptual designs of "commercial" Tokamak power reactors. The parameters for the commercial reactors are in a certain sense a moving target, which will change as information is developed in the Tokamak confinement program and the supporting technology development program. Nevertheless, they are useful in giving some indication of what must be accomplished in the experimental power reactor and demonstration power reactor stages. While one cannot merely interpolate in this table to arrive at parameters for the TEPR, such an interpolation is useful in providing guidance for analysis and in providing a measure of assurance that the objectives and the analysis are plausible.

The objective of demonstrating the feasibility of producing 5 to 50 MW(e) of electrical power, averaged over the operating cycle, imposes requirements on the thermonuclear power output during the burn pulse and on the length of the burn pulse. Refueling needs depend on the confinement time. Requirements on power output and confinement time translate directly into requirements on size. These requirements are developed for an ignition device[a] with reference to the idealized geometrical configuration shown in Fig. 1.

The thermonuclear power during the burn pulse is

$$P = \text{const}\, n^2 \overline{\sigma v}\, V_p \quad , \tag{1}$$

where

V_p = plasma volume

n = D-T ion density

$\overline{\sigma v}$ = Maxwellian-averaged fusion cross section.

The maximum ion density is limited by the constraint on the maximum value of β_θ, the ratio of plasma thermal pressure to the magnetic pressure of the poloidal confining field,

$$n \propto \frac{\beta_\theta I^2}{a^2 T} \quad , \tag{2}$$

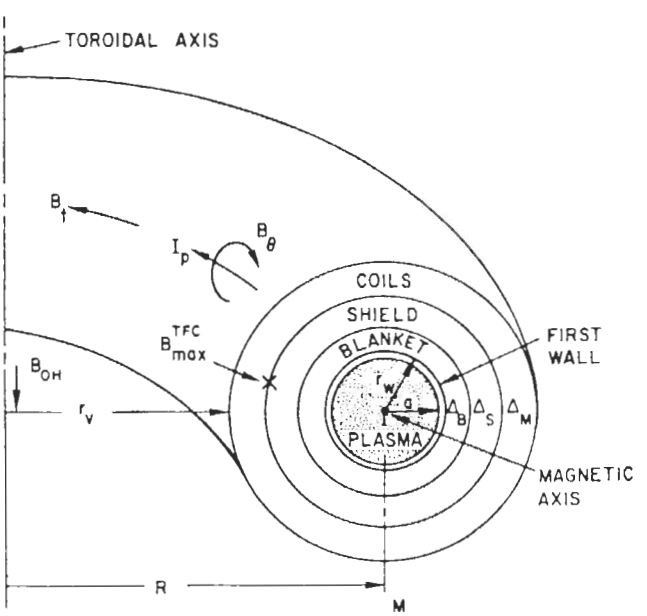

Fig. 1. Idealized Tokamak configuration.

[a] An ignition device is defined as one in which alpha heating is sufficient to maintain the energy balance at the operating condition without resorting to supplemental heating.

TABLE I

TEPR Objectives

General Features
1. Logical next step beyond TFTR in plasma confinement devices.
2. Two distinct stages—an initial stage based largely on current technology and a second stage that demonstrates new breeder-blanket technology.
3. Plasma performance can be demonstrated early in Stage I, before funding decisions on breeder-blanket technology demonstration experiments for Stage II.
4. Blanket-tritium technology demonstration experiments are scheduled to allow time for technology development programs.
5. Electrical power breakeven is demonstrated before 1990 (tentative).
6. Major components designed to accommodate objectives of both stages, as appropriate.
Stage I (~1986 to 1989)
Objectives
1. Study plasma confinement, stability, fueling, heating, and control in the reactor regime.
2. Heat, fuel, and confine a reactor-grade D-T plasma under such conditions that the generation of 5 to 50 MW(e) of electrical power is feasible.
3. Utilize as a materials irradiation facility.
4. Demonstrate certain technologies (e.g., superconducting magnets) in a power reactor environment.
5. Operate an energy conversion blanket with sensible heat removal under such conditions that the generation of 5 to 50 MW(e) of electrical power is feasible.
6. Demonstrate electrical power breakeven (tentative).
Features
1. The plasma physics objective (the first one) can be achieved with a low-temperature blanket.
2. The blanket functions only as an energy convertor, without lithium and the extra complication of tritium extraction and containment.
3. The design and achievement of objectives should be predicated on technology that is either presently available or that can be developed with realistic technology development programs.
4. Adequate supplemental neutral-beam heating will be provided so that the first five objectives can be obtained in the beam-driven mode if plasma confinement is less than anticipated.
Stage II (~1990 to 1995)
Objectives
1 Demonstrate the breeding, extraction, processing, and containment of tritium with a blanket test module operating at low temperature.
2. Demonstrate the breeding, extraction, processing, and containment of tritium with a blanket test module operating at temperatures such that sensible heat is removed and 5 to 50 MW(e) of electrical power production is feasible.
3. Utilize as a test facility to achieve above objectives for alternate blanket modules embodying different primary energy conversion, sensible heat removal, and tritium extraction concepts.
4. Utilize as a materials irradiation facility.
Features
1. Primarily an engineering test facility to demonstrate the required blanket-tritium technology in a power reactor environment.
2. Simultaneous utilization as a component and radiation test facility (to the extent that this is possible).

TABLE II

Tokamak Parameters

	R (m)	a (m)	$A = R/a$	I (MA)	B_t (kG)	n_e (10^{19} m^{-3})	T_i (keV)	T_e (keV)	β_θ	q	τ_E (msec)	P_T (MW)	Operation Date
Existing Experiments (Ref. 4)													
ST	1.09	0.13	8.4	0.07	40	4.0	0.60	2.50	0.8	5.1	10		
ORMAK	0.80	0.23	3.5	0.12	18	3.0	0.30	0.70	0.5	5.0	11		
ATC (uncompressed)	0.90	0.17	5.3	0.06	15	1.5	0.25	1.00	0.4	4.0	5		
ATC (compressed)	0.36	0.11	3.3	0.13	35	8.0	0.75	2.50	0.2	4.0	3		
Doublet II	0.59	0.12/0.15	4.5	0.14	8	1.3	0.25	0.55	0.6	5.0	2		
TFR (Ref. 5)	0.98	0.20	4.9	0.10-0.30	50	4.0	1.00	1.00	0.8	2.8	16		
TM-3	0.40	0.08	5.0	0.07	40	7.0	0.35	0.50	0.8	4.6	3-4		
T-4	1.00	0.17	5.9	0.12	40	4.0	0.70	1.50	0.8	4.8	16		
T-6	0.70	0.25	2.8	0.06	10	1.0	0.20	0.30	0.3	7.4	1		
Next Generation Experiments (Ref. 4)													
T-10	1.50	0.40	3.8	1.1	50		2.0			2.5			1975
PLT	1.30	0.45	2.9	1.6	50	10.0	3.1	3.1	0.3	2.4			1975
Doublet III	1.40	0.45/1.5	3.1	5.0	26	20.0	5.0		1.0	2.6			1978
Feasibility Experiment (Ref. 3)													
TFTR (nominal)	2.50	0.56	4.5	1.0	49	8.0	6.0	6.0	1.0	3.0	200	7.4	1980
TFTR (high current)	2.70	0.95	2.8	2.5	45	13.0	8.5	8.1	>2.0	3.0			
Experimental Power Reactor													
?													
Demonstration Power Reactor													
?													
Commercial Reactor													
PPPL (Ref. 6)	10.5	3.25	3.2	14.6	60	20.0	56	24	1.8	2.1		5000	
UWMAK-1 (Ref. 7)	13.0	5.0	2.6	21.0	38	8.0	11	11	1.1	1.75	1.4×10^4	5000	

where

I = plasma current that produces the confining poloidal field

a = plasma radius

T = plasma temperature.

Theoretically, $\beta_\theta \leq A \equiv R/a$ for plasma equilibrium and magnetohydrodynamic (MHD) stability.[4]

Stability against "kink-mode" MHD plasma oscillations limits the maximum plasma current

$$I \propto \frac{a B_t}{qA} \quad , \tag{3}$$

where q is the safety factor for kink-mode MHD stability. The $q(a) \geq 2.5$ is thought to be adequate for stability.[4]

The maximum field at the toroidal field (TF) coil, B_{max}^{TFC}, is limited by technological constraints on the superconductor. For niobium-titanium, $B_{max}^{TFC} \lesssim 100$ kG, and this must be further reduced to allow for the presence of other fields. The field in the plasma is reduced by a geometrical factor (see Fig. 1)

$$B_t = \frac{r_v + \Delta_m}{R} B_{max}^{TFC} = \left(1 - \frac{r_w + \Delta_B + \Delta_S}{R}\right) B_{max}^{TFC} \quad . \tag{4}$$

Combining these results leads to

$$P \propto \frac{\beta_\theta^2 (B_{max}^{TFC})^4}{q^4} \frac{a^2 R}{A^4} \left(1 - \frac{r_w + \Delta_B + \Delta_S}{R}\right)^4 \frac{\overline{\sigma v}}{T^2} \quad . \tag{5}$$

The quantity, $\overline{\sigma v}/T^2$, depends only on the plasma temperature and has a broad maximum at $T \approx 13$ keV, as shown in Fig. 2. For a fixed aspect ratio, A, an increase in size increases the power in two ways:

1. the plasma volume increases, $P \propto a^2 R \propto R^3/A^2$
2. the field in the plasma increases $P \propto (C_1 - C_2/R)^4$.

To attain a power balance in the plasma during the burn pulse, the power losses (radiation and transport) must equal the power sources (fusion alpha, ohmic, and possibly supplemental heating). The transport loss is inversely proportional to the confinement time, which is characterized by the parameter $n\tau$. The value of $n\tau$ that must be achieved to have a balance can be determined by solving the plasma power and particle balance equations. The required $n\tau$ can be reduced by using supplemental heating (e.g., neutral beams of energetic deuterons). The required $n\tau$ is shown in Fig. 3 for several values of the parameter ξ, which is the ratio of supplemental to fusion alpha heating of the plasma.

The relationship among the required $n\tau$, size, and other reactor parameters depends on the transport mechanism that will govern the energy confinement in the TEPR. What mechanism this will be is not known at this time, although there are theoretical arguments[4,8] that trapped-particle instabilities will govern energy transport in a reactor-type plasma. In particular, the dissipative trapped-ion mode (TIM) instability is thought to be the major energy transport mechanism that will

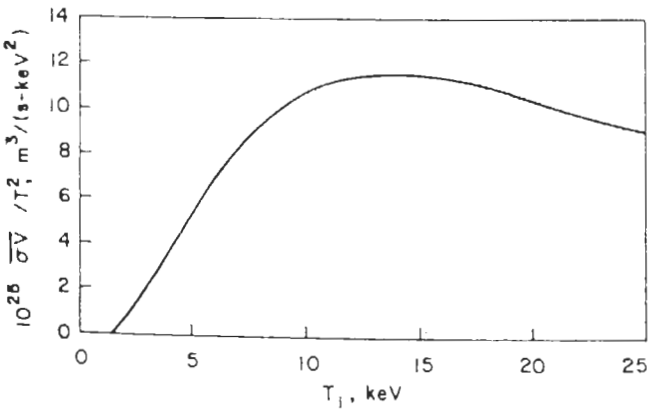

Fig. 2. Fusion reaction parameter, $\overline{\sigma v}/T^2$.

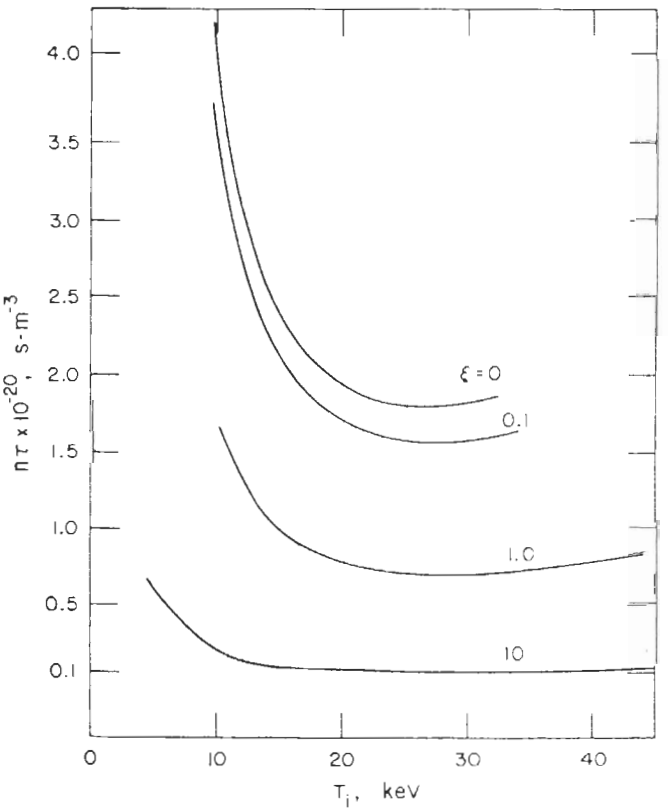

Fig. 3. Confinement.

be present in the TEPR. The TIM theory, when combined with Eqs. (2), (3), and (4), leads to a requirement on the size that is necessary to attain a given $n\tau$.

TIM

$$n\tau \propto \frac{\beta_\theta^2 (B_{max}^{TFC})^6}{q^4 T^{11/2}} \frac{a^4 [1 - (r_w + \Delta_B + \Delta_S)/R]^6}{A^{3/2}} \quad . \quad (6)$$

Although the trapped particle modes are expected to be the most likely energy transport mechanism in the TEPR, on theoretical grounds, current experiments are roughly consistent with ion-energy transport predicted by the neoclassical theory, while electron-energy transport and particle transport seem to follow a pseudoclassical (PC) theory in which the magnitudes of the transport coefficients are somewhat larger than predicted by the neoclassical theory.[4] Thus, extrapolation of current experimental results to the TEPR regime indicates a classical type of energy loss which, when combined with Eqs. (3) and (4), leads to a requirement on the size that is necessary to attain a given $n\tau$.

PC

$$n\tau \propto \frac{(B_{max}^{TFC})^2 T^{1/2}}{q^2} \frac{a^2 [1 - (r_w + \Delta_B + \Delta_S)/R]^2}{A^2} \quad . \quad (7)$$

For a fixed aspect ratio, A, confinement improves with size in two ways:

1. the plasma gets bigger, $n\tau \propto a^m \propto R^m/A^m$
2. the field in the plasma increases, $n\tau \propto (C_1 - C_2/R)^p$, where $m = 4$ and $p = 6$ for TIM, and $m = p = 2$ for PC.

Thus, both power level and confinement increase with size, maximum field at the TF coil, and β_θ (for TIM scaling), and both decrease with the safety factor, q, and the aspect ratio, A. The power level increases with ion temperature up to $T \approx 13$ keV, then decreases. The confinement decreases rapidly ($T^{-11/2}$) with temperature for TIM scaling and increases slowly ($T^{1/2}$) with temperature for PC scaling.

The blanket (Δ_B) and shield (Δ_S) thicknesses are determined by the requirements that the radiation damage to the components of the superconducting TF coils and the radiation heat load to the refrigeration system for these coils be sufficiently low. An analysis of this question is presented in a subsequent section. The conclusion is that $\Delta_B + \Delta_S \approx 1$ m. There is a strong incentive to minimize this thickness because the magnetic field in the plasma varies directly with $(\Delta_B + \Delta_S)/R$, for a given B_{max}^{TFC}, and the power varies as B_t^4.

The thicknesses of the TF coil, of the ohmic-heating (OH) (transformer) coil, and of the central support cylinder are determined from magnet design requirements. Analysis indicates that the combined thickness, Δ_m, should be ≈ 1 m.

The change in magnetic field produced by the OH (transformer) coils, ΔB_{OH}, varies with plasma current, I, major radius, R, and central core radius, r_v, approximately as

$$(\Delta B_{OH})_{ind} \propto \frac{RI}{r_v^2} \propto \frac{a^2 B_{max}^{TFC} [1 - (r_w + \Delta_B + \Delta_S)/R]}{r_v^2 q} . \quad (8)$$

Relation (8) pertains to the field change required to induce the plasma current. Allowing a factor of ~ 2 for plasma resistive losses and a factor of $\sim \frac{1}{2}$ for a superconducting coil going from $-B_{OH}$ to $+B_{OH}$, relation (8) determines the minimum r_v for which $|B_{OH}|$ is less than the limit for niobium-titanium superconductors ($|B_{OH}| \lesssim 100$ kG). For a conventional copper conductor, operation would be from $-B_{OH}$ to 0, so the minimum r_v would be that for which ΔB_{OH} was less than one-half the limit for copper conductors ($\Delta B_{OH} \lesssim 60$ kG).

Noncircular plasma cross sections promise some advantage relative to circular plasma cross sections in terms of the power level and confinement for a given reactor size. For a noncircular plasma with minor dimension a (dimension in the horizontal midplane in Fig. 1), a factor, l, is defined as the ratio of the circumference of the noncircular plasma to the circumference of a circular plasma with radius, a, and a factor, κ, is defined as the ratio of the cross-section area of the noncircular plasma to a circular plasma with radius a {e.g., for an elliptical cross section, with major radius b, $\kappa \approx b/a$, and $l \approx [\frac{1}{2}(1 + \kappa^2)]^{1/2}$}. Relations (2) and (3) obtain for the noncircular plasma, but with a replaced by al (including in $\bar{A} \equiv R/al$), and Eq. (4) is unchanged. Thus, for a noncircular plasma, the thermonuclear power scales as

$$P \propto \frac{\beta_\theta^2 (B_{max}^{TFC})^4}{q^4} a^2 \kappa R \left(\frac{al}{R}\right)^4 \left(1 - \frac{r_w + \Delta_B + \Delta_S}{R}\right)^4 \times \frac{\overline{\sigma v}}{T^2} \quad , \quad (9)$$

which reduces to relation (5) for $l = \kappa = 1$. If noncircular cross-section plasmas can operate at the same β_θ and q as circular cross-section plasmas, a point that is uncertain but that should be resolved by the Doublet-III experiments, the former should realize a significant advantage over the latter in power performance. This advantage arises primarily because a given volume of plasma can be located closer to the inside of the TF coil, and hence it is in a higher magnetic field, if it is noncircular, than if it is circular.

Relations (6) and (7) also are assumed to apply to noncircular plasma cross sections, when a is replaced by al, although there may be other differences in confinement scaling. As was the case with power output, confinement is improved by the stronger magnetic field in the plasma, which allows a larger plasma current.

Impurities have an important effect on the power balance in Tokamaks, particularly on ignition devices. High-Z ions sputtered or outgassed from the first wall enhance the radiation loss from the plasma, and the significance of this plasma contamination on the power balance depends strongly on the atomic number of the impurity ion. Using the computational model that is described in Ref. 2, the minimum temperature for which ignition occurs (the temperature below which the radiation loss exceeds the alpha heating) was determined for several impurity species. These results are plotted in Fig. 4 as a function of the impurity concentration in the plasma. Oxygen is a typical background gas, carbon and silicon would be found in a device with a graphite or silicon-carbide surface, iron would be found in a device with a stainless-steel first wall, and molybdenum is representative of the higher-Z materials that might be used for first walls or limiters. The D^+ and T^+ sputtering coefficients are $\sim 5 \times 10^{-3}$ atom/ion, so that an impurity concentration on this order could be anticipated in a device that operated for several particle confinement times without special impurity control measures. Considering that the confinement predicted by TIM theory decreases with temperature as $T^{-11/2}$, it is unlikely that an ignition device could be operated with a stainless-steel first wall without special impurity control measures. On the other hand, ignition devices with low-Z material (e.g., beryllium, boron carbide, silicon-carbide, or graphite) first-wall surfaces should be possible for $T = 10$ keV.

The power that would be obtained during the peak portion of the burn pulse is plotted as a function of major radius, R, in Fig. 5, for $T = 10$ keV. Results are shown as a function of aspect ratio for circular ($\kappa = 1$) and noncircular ($\kappa = 3$) plasmas. These results indicate the size reactor that is required to obtain a given power, without regard for the question of confinement, for the parameters ($q = 2.5$, $\beta_\theta = 2.2$, $\Delta_B + \Delta_S = 1$ m, $B_{\max}^{TFC} = 75$ kG). Some of the smaller devices indicated in Fig. 5 would not be allowed because the central core radius, r_v, is so small that $|\Delta B_{OH}|$ is excessive. Allowing a factor of $\sim\frac{1}{2}$ for pulsed operation, the TEPR power objective [5 to 50 MW(e)] should be comfortably satisfied by a reactor with $P \approx 100$ MW(th) during the burn pulse. For an aspect ratio of 3, this requires $R \approx 6$ m for a circular plasma and $R \approx 5$ m for a $\kappa = 3$ noncircular plasma.

The discussion up to this point has focused on ignition devices, although driven devices, in which

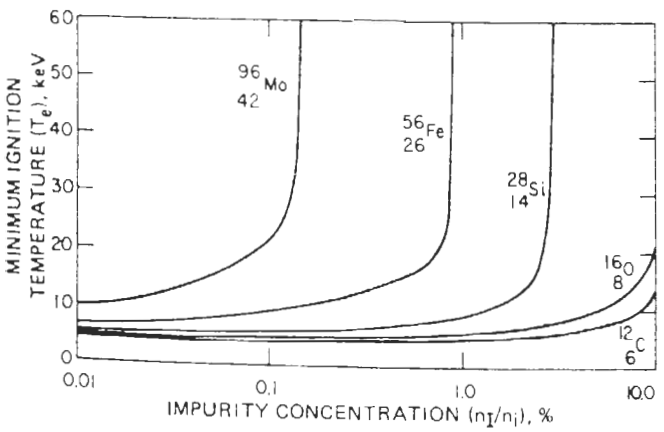

Fig. 4. Effect of impurities on ignition.

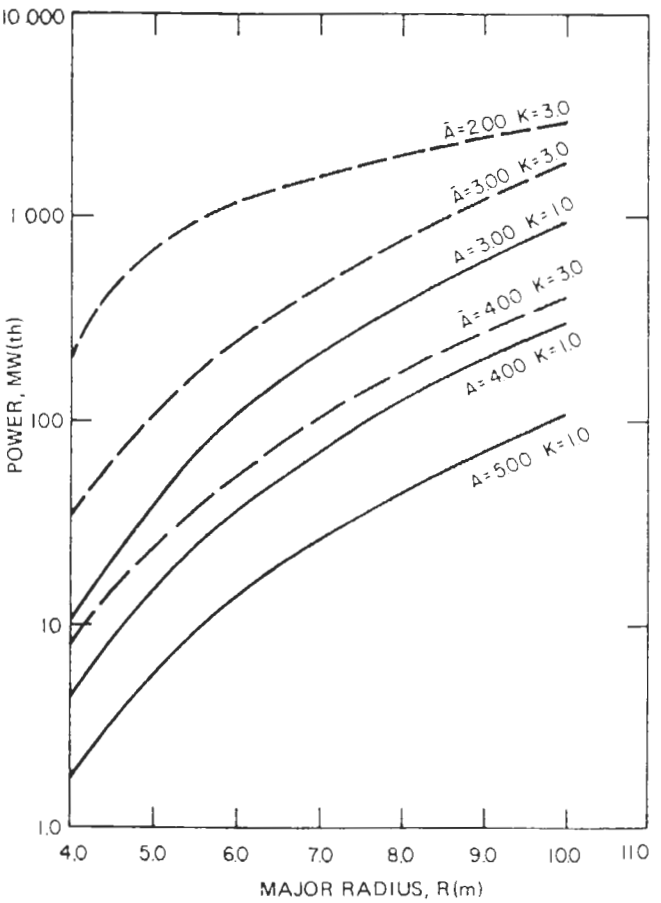

Fig. 5. Power versus size ($B_{\max}^{TFC} = 75$ kG, $\beta_\theta = 2.2$, $q = 2.5$, $T = 10$ keV).

the alpha heating is supplemented by neutral-beam (D_0) injection heating, are also considered in this study. Similar analyses for devices driven to $Q_{plasma} \approx 10$, which is about the lowest value for which net electrical power is conceivable, indicate that the values of R cited in the preceding paragraph could be reduced slightly.

The experimental basis for confidence in the noncircular plasma cross section is not nearly as extensive as for the circular plasma cross section. However, the predicted size advantage associated with the noncircular cross section is significant. The Doublet-III program is intended to provide an experimental confirmation that this advantage can be realized. In this study, the performances of circular and noncircular cross-section plasmas, which would fit into the same TF coil systems, are evaluated in parallel, but the technological systems are sized to be compatible with the circular cross-section plasma.

IV. PRELIMINARY CONCEPTUAL DESIGN SUMMARY

On the basis of trade-off studies among the plasma-power objectives and uncertainties, the TF coil design, the plasma heating and driving systems requirements, the radiation and energy attenuation requirements and access considerations, a reference point was selected for the development of the engineering design. This reference point was sized on the basis of a circular plasma cross section. A $\kappa = 3$ (3:1) noncircular plasma design utilizing the same TF coil system and having the same plasma volume was developed in parallel, but in less detail.

A perspective view of the TEPR reference design is shown in Fig. 6, for the circular plasma, and the geometrical parameters are tabulated in Table III. A vertical section view is presented in Fig. 7 for the circular design.

The plasma properties during the peak, quasi-steady-state portion of the burn cycle are given in Table IV. The maximum field, B_{max}^{TFC}, at the TF coils is 75 kG in the primary design. However, a design option with $B_{max}^{TFC} = 100$ kG is being considered. These properties are for operation at ignition, which requires energy confinement ten times that predicted by TIM for the circular plasma and five times TIM for the noncircular plasma, with $B_{max}^{TFC} = 75$ kG, and two times TIM for the circular plasma with $B_{max}^{TFC} = 100$ kG. If the achievable energy confinement turns out to be less than this, the reactor will be operated in a beam-driven mode to achieve essentially the same properties. The noncircular plasma design has a more conservative value of $q(a)$ than the circular design does—the power output of the noncircular design would be substantially greater if operated at $q(a) = 2.5$.

The power performance of the TEPR and the

TABLE III

TEPR Preliminary Conceptual Design Geometrical Parameters

Central core radius, r_v	1.8 m
Thickness of TF coil + OH coil + support cylinder, Δ_m	1.05 m
Blanket + shield thickness, inside, $\Delta_B^{in} + \Delta_S^{in}$	1.0 m
TF coil minor bore, R_{bore}	7.7 m
TF coil major bore, Z_{TFC}	11.9 m

Circular Plasma		Noncircular Plasma ($\kappa = b/a = 3$)	
Plasma radius, a	2.1 m	Plasma minor dimension, a	1.3 m
First-wall radius, $r_w = a + \Delta_v$	2.4 m	First-wall minor dimension, $r_w = a + \Delta_v$	1.6 m
Major radius, R	6.25 m	Major radius, R	5.45 m
Aspect ratio, $A = R/a$	2.98	Aspect ratio, $\bar{A} = R/al$	1.9
Plasma volume	544 m^3	Plasma volume	545 m^3
Toroidal vacuum chamber volume	711 m^3	Toroidal vacuum chamber volume	826 m^3
First-wall area	592 m^2	First-wall area	770 m^2
Blanket + shield thickness, outside, $\Delta_B^{out} + \Delta_S^{out}$	1.3 m[a]	Blanket + shield thickness, outside, $\Delta_B^{out} + \Delta_S^{out}$	1.3 m[a]

[a]Blanket and shield thickness = 1.3 m. The space available within the TF coil is 1.9 m for the circular plasma and 3.5 m for the noncircular plasma.

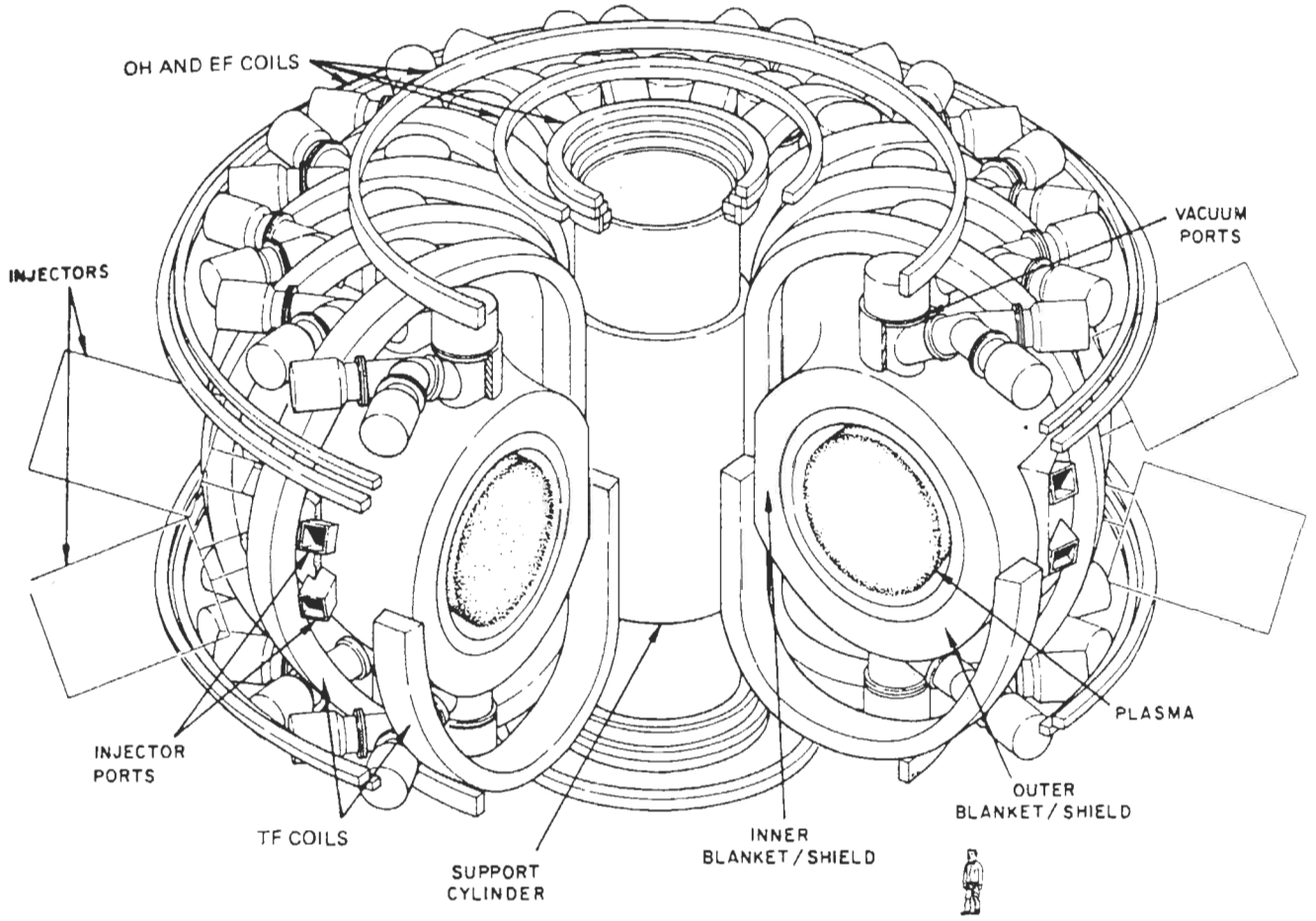

Fig. 6. TEPR perspective view.

requirements on the plasma driving and heating systems are summarized in Table V for the circular plasma design. The plasma is heated ohmically during the current rise, but 40-MW supplemental neutral-beam (D) heating is required to reach operating temperature. If energy confinement is adequate for ignition, the beam heating is terminated once the operating temperature is achieved; otherwise a supplemental heating beam is used to maintain the power balance during the burn phase. A constant plasma density is maintained during the startup and burn phases by plasma refueling and recycling. The burn-cycle length will be determined by the length of time that a stable plasma can be confined or by the buildup of impurities. Burn cycles in the range of 10 to 60 s are analyzed, but the plasma-driving system is adequate for much longer burn cycles. The cycle-average electrical power (assuming a thermal-to-electrical conversion efficiency of 0.3) is relatively insensitive to the confinement, but the cycle-average, net-electrical power (assuming an efficiency of 0.5 for beam production and an efficiency of 0.95 for the plasma-driving system power supply) is positive only if the confinement is adequate for, or very close to, ignition. Sputtering from a stainless-steel first wall would extinguish the plasma and preclude a reasonable power performance. The power performance is only slightly degraded from that indicated in Table V if the first wall is coated with a low-Z material such as graphite, but a silicon-carbide or aluminum first-wall surface results in shorter burn cycles and degraded power performance. The power performance shown in Table V is based on a conservative value of $B_{max}^{TFC} = 70$ kG—using the design value of $B_{max}^{TFC} = 75$ kG increases $\overline{P}_E$ by $\approx 30\%$ and has a corresponding beneficial effect on $\overline{P}_{NET}$.

A secondary function of the TEPR is to serve as a radiation facility. The TEPR was sized, using a plausible set of design parameters, to obtain the objective of a rather modest amount of power, with the result that the 14-MeV neutron power load on the first wall is also rather modest,

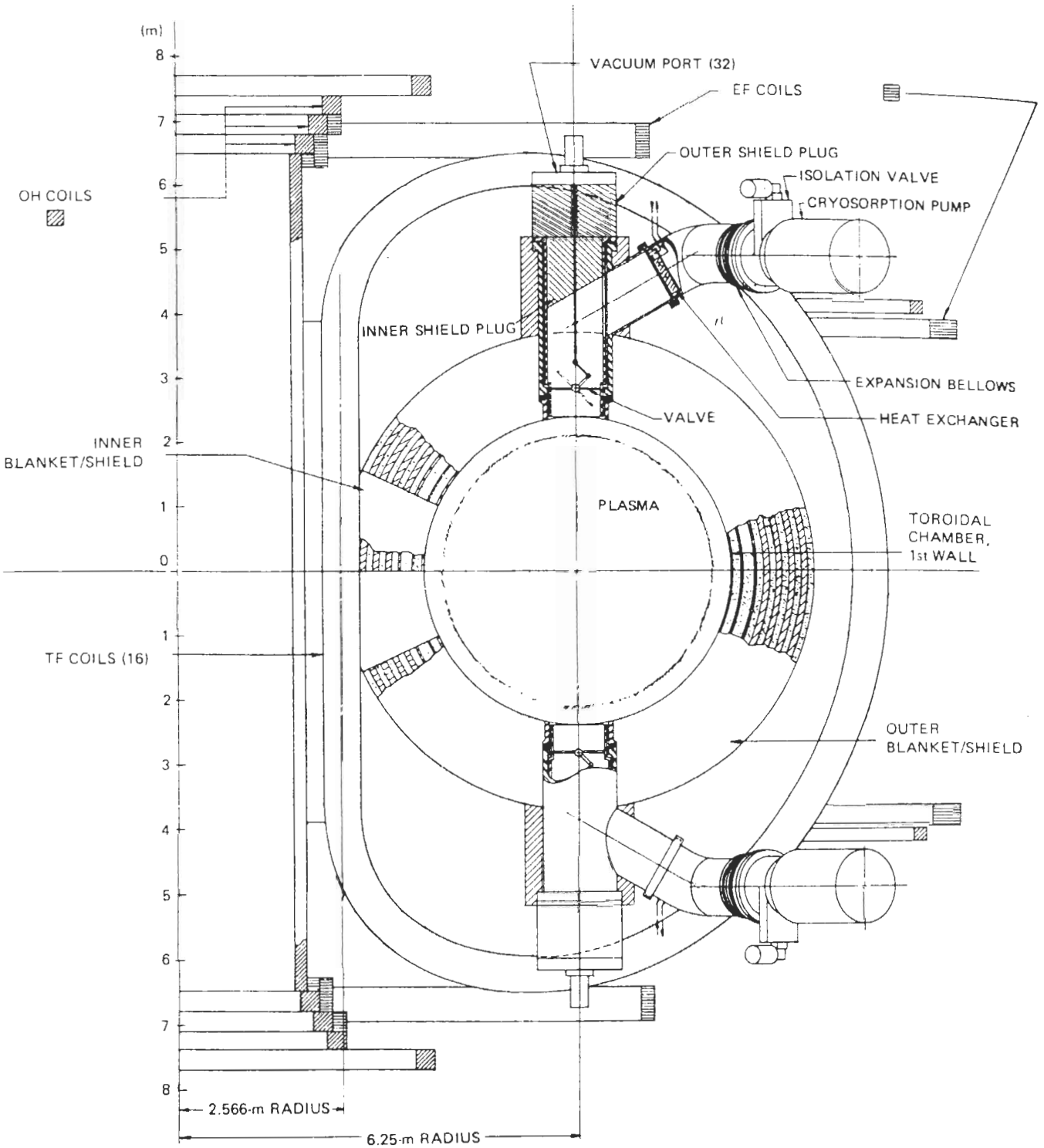

Fig. 7. TEPR vertical section—circular plasma.

which is an advantage from the viewpoint of radiation damage to the reactor, but is a disadvantage in terms of using the TEPR as a radiation facility. To obtain some indication of the maximum possible neutron-flux achievable in the TEPR, an optimistic set of parameters [$q(a) = 2.5$, $\beta_\theta = 3.5$, $B_{max}^{TFC} = 80$ kG] was considered. If the TEPR could operate with these parameters, it would serve quite well as a radiation facility, with neutron wall loads of $P_w \approx 0.5$ MW/m^2 for the

TABLE IV

TEPR Steady-State Plasma Properties at Equilibrium

Parameter	B_{max}^{TFC} = 75 kG		B_{max}^{TFC} = 100 kG
	Circular Plasma $\kappa = 1$	Noncircular Plasma $\kappa = 3$	Circular Plasma $\kappa = 1$
Pressure ratio, β_θ	2.2	2.0	2.2
Safety factor, $q(a)$	2.5	4.0	2.5
Density, n_i (m^{-3})	0.56×10^{20}	0.65×10^{20}	0.99×10^{20}
Temperature, T_i (keV)	9.6	9.6	9.6
T_e (keV)	10.0	10.0	10.0
Confinement, $n\tau$ (s/m^3)	4.2×10^{20} (10 × TIM)	4.2×10^{20} (5 × TIM)	4.2×10^{20} (2 × TIM)
Plasma current, I_p (MA)	4.8	7.6	6.4
Toroidal field, B_t (kG)	34	39	46
Power, P_T [MW(th)]	129	174	409
Neutron-wall load, P_w (MW/m^2)	0.16	0.17	0.51

TABLE V

TEPR Burn Cycle Performance—Circular Plasma

Burn Cycle		
Current rise phase (s)		1
Beam heating phase (s)		~3
Burn phase (s)		20-50
Shutdown phase (s)		5
Exhaust and replenishment phase (s)		~15
Neutral-Beam Requirements		
Startup = 40 MW @ 180 keV for ≈3 s		
Burn[a] = 23 MW @ 180 keV for 20 to 50 s		
Plasma Driving System Requirements		
$\Delta\phi$ (V-s)		~100
Peak power [MW(e)]		~1000
Energy (MJ)		~450
Reactor Performance (B_{max}^{TFC} = 70 kG)	$n\tau$ = 15 × TIM	$n\tau$ = TIM
Electrical power, $\bar{P}_E$ [MW(e)]	~25	~25
Net electrical power, $\bar{P}_{NET}$ [MW(e)]	15-20	~-17

[a]Required if $n\tau$ = TIM.

circular plasma design and $P_w \approx 4$ MW/m^2 for the noncircular plasma design. Also, with B_{max}^{TFC} = 100 kG, $P_w \approx 0.5$ MW/m^2 for the circular plasma design.

Cryogenically stable superconducting TF, OH, and equilibrium field (EF) coils are proposed for the TEPR, although conventional copper coils are still under consideration for the latter two sets of coils. The magnet-system characteristics are given in Table VI. The superconducting material is niobium-titanium, with a copper stabilizer and a stainless-steel support structure. There are 16 pure-tension D-shape TF coils, which provide an access between coils of ~3 m with a maximum field ripple of ~2%. The average current density is 1280 A/cm^2, which produces a peak field of 75 kG at the inside of the D. This value of 75 kG was chosen to allow ~5-kG stray fields from other magnet systems and from fields due to the plasma current without exceeding the ~80-kG limit for niobium-titanium at 4.2 K. The maximum hoop-stress level in the support system for the TF coils is ≲24 000 psi, and the stored energy is <1000 MJ per coil.

Both the OH and the EF coils are located external to the TF coils. This arrangement has certain advantages with respect to reduced radiation and thermal loads, ease of assembly, reduced pulsed fields on the steady-state TF coils, and ease of producing the required vertical field. The disadvantage of this location is poorer coupling to the plasma. These two sets of coils are capable of producing 110 V-s in the plasma, with one-third of this being produced by the EF coils.

The performance requirements for the neutral-beam injection system are summarized in Table VII. Ion-source currents (total, not per source) are given for injection of all three components (D^+, D_2^+, D_3^+) and for injection of only the D^+ component. An injection system consisting of 16 or 32 injectors, with counter- and co-injection in the horizontal midplane and each capable of delivering 2.5 or 1.25 MW, would satisfy these requirements. Details of the injection system will be based on positive-ion sources of the type presently under active development.

Toroidal chamber and neutral-beam system vacuum requirements are indicated in Table VIII. The toroidal vacuum system was sized to pump down from 10^{-3} to 10^{-5} Torr during the ~15-s

TABLE VI

TEPR Magnet System Characteristics

TF Coils	
Superconductor/stabilizer/ support	NbTi/copper/stainless steel
Number of coils	16
Shape	pure-tension D
Major bore (vertical)	11.9 m
Minor bore (horizontal)	7.7 m
Field in plasma, B_t	34 kG
Peak field, B_{max}^{TFC}	75 kG
Current density, J_{av}	1280 A/cm^2
Operating temperature	4.2 K
Ampere turns	6.54×10^6 per coil 104.6×10^6 total
Stored energy	15 600 MJ
Maximum hoop stress in stainless-steel support	≈ 24 000 psi
Maximum field ripple	≈ 2%
Access between coils	3 m
EF Coils	
Superconductor/stabilizer	NbTi/copper and cupronickel
Current density, J_{av}	2300 A/cm^2
Equilibrium field in plasma	3.0 kG
Ampere turns	10×10^6
Stored energy	900 MJ
V-s to plasma	37 V-s
Peak field	37 kG
Field rise in conductor	37 kG/s
OH Coils	
Superconductor/stabilizer	NbTi/copper and cupronickel
Current density, J_{av}	1280 A/cm^2
Peak field, B_{OH}	32 kG
Ampere turns	45×10^6
Stored energy	883 MJ
V-s to plasma	73 V-s
Field rise in conductor	64 kG/s

TABLE VII

Neutral-Beam Injection System Requirements (Nominal)

Heating	
Injected power (total)	40 MW
Ion-beam composition	75% D^+, 18% D_2^+, 7% D_3^+
Ion-source current	890/1600 A[a]
Ion-source power	160/290 MW[a]
Ion-beam energy	180 keV
Pulse duration	3 s
Number of injectors	16-32
Suplemental Heating (Beam-Driven Mode)	
Injected power	23 MW
Ion-beam composition	75% D^+, 18% D_2^+, 7% D_3^+
Ion-source current	510/920 A[a]
Ion-source power	92/170 MW[a]
Ion-beam energy	180 keV
Pulse duration	20-50 s
Number of injectors	16-32

[a] D^+, D_2^+, D_3^+ injection/D^+ injection.

TABLE VIII

TEPR Vacuum Systems

Toroidal Vacuum System	
Volume	711 m^3 (897 with duct)
Surface area	592 m^2 (1528 with duct)
Gas load after burn	704 Torr-ℓ (888 with duct)
Number of pumping ports	32
Diameter of port	0.914 m
Number of cryosorption pumps	32 (64 for on-line regeneration)
Pump speed	25 000 ℓ/s (rated)
Pumpdown time 10^{-3} to 10^{-5} Torr	14 s (with duct)
Secondary pumps	
Number of 1300-CFM blower stations	16
Number of 1400-ℓ/s turbo pumps	16
Neutral-Beam Vacuum System	
Number of beams	16 minimum
Gas load/beam	21 Torr-ℓ/s[a]
Pumping speed/beam	200 000 ℓ/s[a]
Number of cryosorption panels	4 per beam[a]
Pump size	1 m^2 cryosurface per 50 000 ℓ/s

[a] 16 injectors and 3-component (D^+, D_2^+, D_3^+) injection.

exhaust phase between burn pulses and to achieve ~10^{-9}-Torr base pressure following a ~24-h bake at 400°C at the beginning of an experimental period. The neutral-beam vacuum system was sized to handle the gas load that would be required in each beam for 40 MW of injected power.

The energy storage and transfer portion of the OH system power supply is a major design concern, since the energy of the coil of ~10^9 J must be transferred out of and back into the coil in a period of one second. The peak powers approach 3000 MW. The maximum voltage and current that must be handled are ~140 000 V and ~40 000 A, respectively. Conventional energy storage systems will be too costly or inefficient.

Homopolar generators are attractive with respect to high peak powers and large energy storage for a relatively low price. However, the conventional homopolar generator is a poor impedance match—being primarily a low-voltage high-current device. Many homopolar generators must be connected in series to develop the necessary coil voltage. An arrangement of concentrically stacked drum-type homopolar generators is being studied for this application.

The characteristics of the primary-energy conversion system (PECS) are outlined in Table IX, a vertical section view of the blanket and shield arrangement is shown in Fig. 8, and the performance of the PECS is summarized in Table X. A stainless-steel first wall with a low-Z coating interfaces with the plasma. Alternating zones of

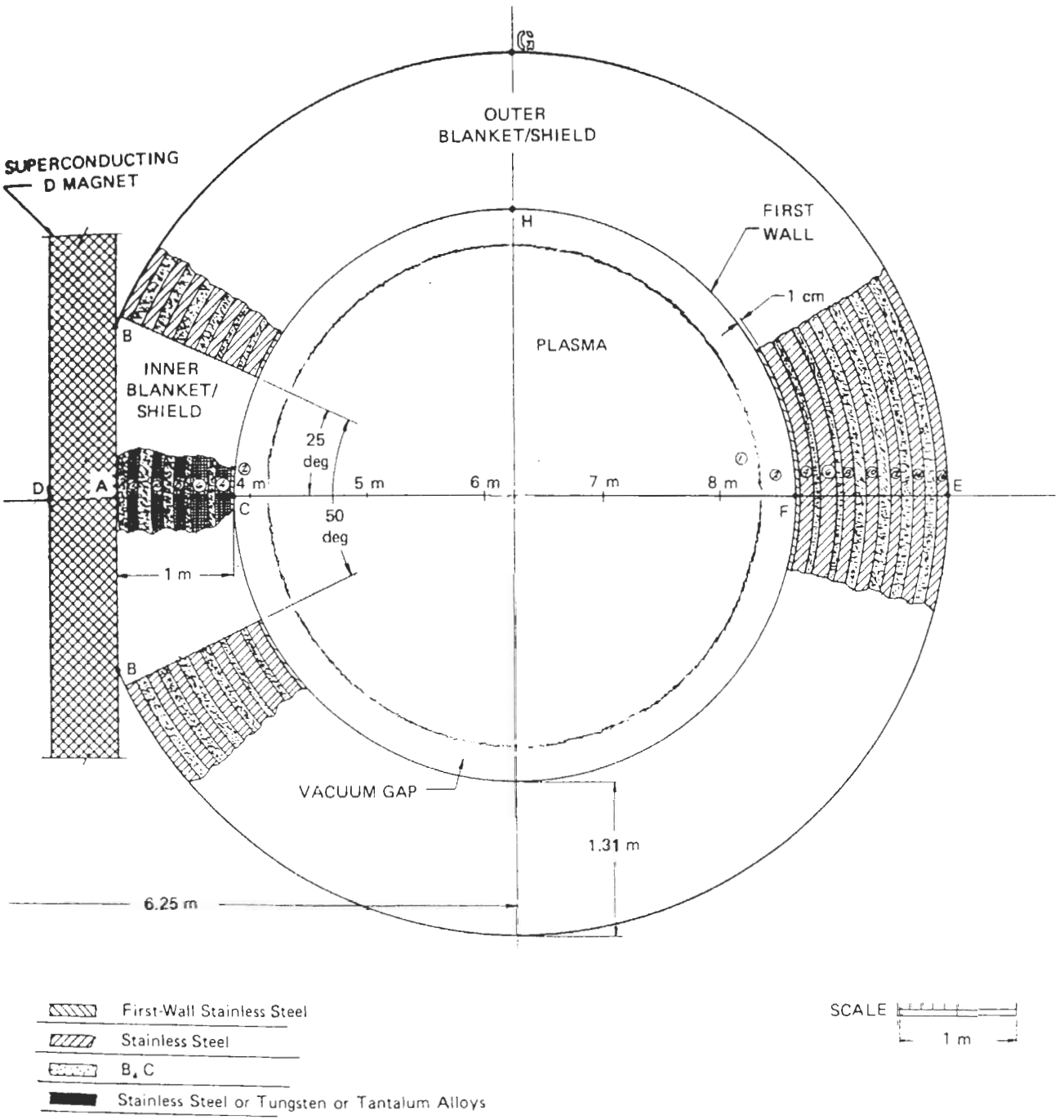

Fig. 8. TEPR blanket/shield vertical section view.

stainless steel and boron-carbide constitute the blanket and shield in the primary design. An alternate design, in which the inner blanket/shield consists of alternating zones of a tungsten- or tantalum-base alloy and boron-carbide to enhance the radiation attenuation, is also considered. The dimensions and compositions of the alternating zones are optimized to maximize radiation attenuation for 1 m of the primary (stainless-steel–B_4C) inner blanket-shield design.

Ninety-nine percent of the nuclear heating occurs in the first 0.4 m of the blanket/shield. The nuclear heating in the superconducting TF coils is comparable to the non-nuclear heat leaks and causes a maximum temperature rise in the superconductor that is <0.05 K.

TABLE IX

TEPR Primary Energy Conversion System

Blanket and shield thickness	
inside	1.0 m
outside	1.3 m
Blanket and shield composition	
inside	stainless steel–B_4C or tungsten alloy–B_4C or tantalum alloy–B_4C
outside	stainless steel–B_4C
First wall	2-cm stainless steel (50% density), ~100 μm of beryllium, BeO, B_4C, SiC, or carbon coating
Coolant	
H_2O (136 atm)	
T_{in}	38°C
T_{out}	302°C
Helium (50 atm)	
T_{in}	357°C
T_{out}	527°C

TABLE X

TEPR Primary Energy Conversion System Performance

First-wall neutron loading (PECS design value[a])	0.2 MW/m^2
Nuclear heating, maximum	
first wall	2.1 W/cm^3
blanket	2.0 W/cm^3
shield	2×10^{-2} W/cm^3
magnet (TF coil)	5×10^{-6} W/cm^3
Nuclear energy deposition rate in TF coil	
per coil	16 W
total (16 coils)	256 W
Maximum radiation-induced resistivity in copper stabilizer of TF coil (10 MW-yr/m^2)	2.5×10^{-8} Ω-cm
Maximum decrease in critical-current density in TF coil superconductor (10 MW-yr/m^2)	<5%
Maximum blanket temperature	≤550°C
First-wall temperature	≤550°C
Coolant pumping power (blanket only)	
H_2O	≪1 MW
helium	~7 MW

[a]The PECS design neutron-wall loading used in the PECS performance evaluation is 25% larger than the nominal design value, for conservatism.

The TF coil is designed to accommodate an increase in resistivity of the copper stabilizer, due to irradiation, of 2.5×10^{-8} Ω-cm. Allowing a factor of 10 for safety, the primary-shield design would allow the TEPR to operate to an integrated neutron wall load of 1 MW-yr/m^2, which corresponds to a 0.2 MW/m^2 wall load for 10 yr with a duty factor of 50% before this criterion was violated, at which time annealing would be necessary.

Sensible heat removal from a blanket operating at T_{max} = 550°C with either water or helium as a coolant is feasible. With helium, average void fractions of 5% in the blanket region and 2% in the shield are required, and ~7 MW(e) is required to pump the coolant through the blanket. Neither coolant volume fraction nor pumping power are significant with water.

First-wall and TF coil radiation damage parameters are given in Table XI. A stainless-steel first wall is expected to maintain its structural integrity for integrated wall loadings in excess of 1 MW-yr/m^2, which would permit over 10 yr of operation at 0.2 MW/m^2 with a duty factor of 50%; <5% swelling[9] and a uniform ductility of over 1% (Refs. 10, 11, and 12) are expected for annealed material. Wall erosion by sputtering and blistering will not seriously affect the mechanical integrity of a stainless-steel first wall under the anticipated particle currents; however, the plasma contamination will be excessive. Further work is necessary to develop a low-Z coating on stainless steel that will withstand the severe radiation, thermal, and chemical environment of the TEPR. The major radiation-damage effect on the TF coils is to increase the electrical resistivity in the copper stabilizer. Adequate shielding has been provided in the design to limit this effect to an acceptable level.

A preliminary study has been carried out to establish criteria for the design and operation of an integrated facility that meets the tritium-handling requirements of a TEPR. For purposes of assessment, the tritium-handling facility for

TABLE XI

Radiation Damage in TEPR

First Wall (maximum)	
Displacements	11 dpa/(MW-yr/m^2) 1.1 dpa/yr[a]
Helium production	216 appm/(MW-yr/m^2) 22 appm/yr[a]
Hydrogen production	531 appm/(MW-yr/m^2) 53 appm/yr[a]
Erosion	~0.1 mm/yr[a]
TF Coil (maximum)	
Displacements in copper	1.5×10^{-5} dpa/(MW-yr/m^2) 1.5×10^{-6} dpa/yr[a]
Neutron fluence	2.36×10^{16} n/cm^{2}[a,b]
Absorbed dose in Mylar	4.0×10^{7} rad/(MW-yr/m^2)

[a]0.2 MW/m^2 neutron-wall load and 50% duty factor.
[b]For 5-yr operation.

Stage I operation has been broken down into six major systems, which provide for fuel delivery, fuel circulation, fuel processing, fuel storage, in-plant containment, and purge processing. Stage II operation requires all six of these systems plus an additional system to provide blanket processing. Table XII contains a summary of preliminary fuel-cycle operating parameters for the TEPR design approach summarized in this section.

V. REACTOR PERFORMANCE

The performance of the TEPR will depend on a number of plasma-physics factors that are uncertain at this time. Foremost among these are the energy confinement and the impurity concentration that will exist in a reactor-grade plasma and the MHD-stability characteristics, particularly of noncircular cross-section plasmas. An envelope of performance characteristics was established to bracket these uncertainties, then a reference design point was selected for more detailed performance analyses and for the engineering design of the TEPR.

To establish the performance envelope, a series of steady-state operating conditions (corresponding to the steady-state portion of the burn pulse) were determined as a function of achievable energy confinement and impurity concentration. In these calculations, B_{max}^{TFC} = 70 kG, β_θ = 2.2, and q = 2.5. Supplemental neutral-beam (D) injection heating was utilized when the energy confinement was inadequate for ignition. The results are summarized, for a relatively clean plasma, in Fig. 9. The total thermal power, P_T, the supplemental beam power, P_B, the neutron wall load, P_W and J_W, and the plasma power amplification factor, Q_P, are plotted as a function of $n\tau$ for the D-T mixture that optimizes each quantity. Ignition requires $n\tau \gtrsim 4 \times 10^{20}$ s/m^3 and net-electrical power production probably requires $n\tau \gtrsim 3 \times 10^{20}$ s/m^3, for a relatively clean plasma. The presence of impurities increases the values of $n\tau$ that are required for these two conditions and may preclude their being obtained, if the impurity is of high enough Z and/or is present in sufficient concentration. However, production of thermal-power output during the burn pulse in the range ~100 to 300 MW(th), with a corresponding neutron wall load of ~0.1 to 0.3 MW/m^2, can be achieved over a range of possible values of $n\tau \gtrsim 10^{19}$ s/m^3, with supplemental heating. Allowing a factor of $\frac{1}{3}$ reduction for thermal-to-electrical conversion and a factor of $\frac{1}{2}$ reduction for burn-cycle duty factor, the TEPR power objective [5 to 50 MW(e)] should be achieved. This power production capability is greater for values of $B_{max}^{TFC} > 70$ kG and for noncircular plasma cross sections. It is relatively unaffected by the presence of impurities, if adequate supplemental heating is provided.

Steady-state performance parameters for a circular and a noncircular reference design are shown in Table XIII. The ratio, α_{TIM}, by which the reactor confinement must exceed the TIM prediction and the plasma power amplification factor, Q_P, are given for a range of confinements. The total thermal power, P_T, the supplemental beam power, P_B, and the neutron wall load, P_W, are

TABLE XII

Fuel Cycle Parameters for the Preliminary TEPR Design

Assumed cycle-average power	100 MW(th)
Tritium burnup rate	16 g/100 MW(th)-day
Deuterium burnup rate	11 g/100 MW(th)-day
Maximum throughput to burnup ratio	100/1
Fuel insertion rate	2700 g/100 MW(th)-day
Maximum fueling costs for a 30% plant factor	
for tritium	$15 M/yr
for deuterium	$5 K/yr
Gross tritium inventory[a]	2 to 4 kG

[a]Largely dependent on fuel cycle turnaround times.

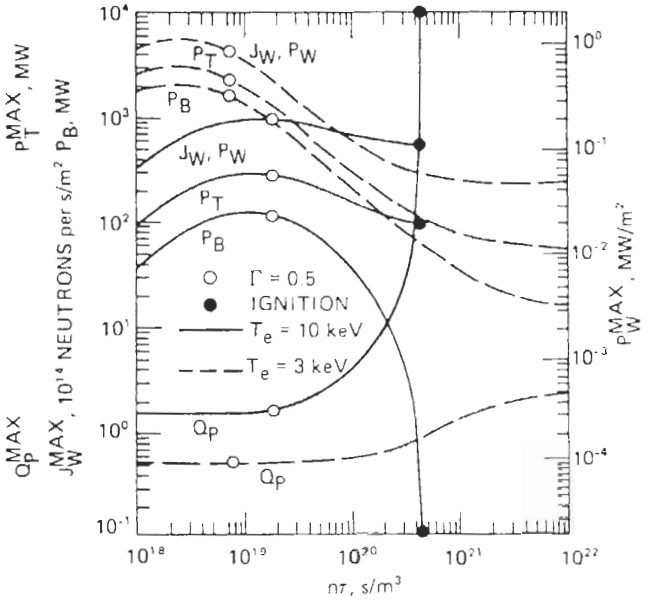

Fig. 9. Several performance parameters of the TEPR as a function of $n\tau$ for 0.5% ^{16}O impurity (q = 2.5, β_θ = 2.2).

TABLE XIII

Equilibrium Performance Characteristics

Q_p	$n\tau$ (10^{20} s/m^3)	α_{TIM}	I (MA)	$\Delta\phi_{ind}$ (V-s)	n_i (10^{20} m^{-3})	T_i (keV)	P_T (MW)	P_B (MW)	P_w (MW/m^2)
(Circular plasma - $\beta_p = 2.2$, $q = 2.5$, $Z_{eff} = 1.3$, $T_e = 10$ keV, $B_{max}^{TFC} = 75$ kG)									
Ignition	4.2	10	4.8	54	0.56	9.6	129	0	0.16
6.5	1.7	5	4.8	54	0.54	10.2	171	23	0.18
1.0	0.057	3	4.8	54	0.16	19.6	294	146	0.18
($\kappa = 3$ noncircular plasma - $\beta_p = 2.0$, $q = 4.0$, $Z_{eff} = 1.3$, $T_e = 10$ keV, $B_{max}^{TFC} = 75$ kG)									
Ignition	4.2	5	7.6	63	0.65	9.6	174	0	0.17
6.5	1.7	2	7.6	63	0.62	10.2	230	31	0.19
1.0	0.057	2	7.6	63	0.18	19.6	395	196	0.19

shown. At ignition, the reference circular-plasma cross-section design produces a thermal-power output of 129 MW(th) and a neutron wall load of 0.16 MW/m^2 during the peak of the burn pulse. Larger power outputs would be obtained in a beam-driven mode, if the confinement turns out to be insufficient for ignition, and for the $\kappa = 3$ noncircular plasma cross-section design. A plasma-driving system that produced ≈100 V-s would provide an ample margin for plasma resistive losses in addition to the $\Delta\phi_{ind}$ needed to induce the plasma current.

The burn-cycle dynamics of the TEPR were examined in some detail. The circular plasma design, but with $B_{max}^{TFC} = 70$ kG and $P_T = 98$ MW to be pessimistic, was analyzed to obtain a lower bound on the power performance. The basic burn cycle consisted of:

1. a 1-s current-rise phase
2. an ~3-s heating phase with 40 MW of neutral deuteron beams
3. a burn phase of variable length
4. a 5-s shutdown phase.

The cycle-average electrical power output, $\overline{P}_{NET}$, computed on the basis of a thermal-to-electrical conversion efficiency of 0.3, and the cycle-average net electrical power, $\overline{P}_{NET}$, accounting for the neutral beam being produced with an efficiency of 0.5 and for the plasma-driving system power supply functioning with an efficiency of 0.95, are shown in Fig. 10 as a function of the length of the burn cycle. If the confinement is sufficient for ignition at $T_e = 10$ keV ($\alpha_{TIM} = 15.2$), $\overline{P}_{NET} \gtrsim 20$ MW(e) is possible for burn cycles of ≈45 s or more. (Down time between burn pulses and power needed for coolant pumping, refrigeration, etc., would reduce $\overline{P}_{NET}$.) If the confinement turns out to be TIM ($\alpha_{TIM} = 1$), then operation at $T \approx 6$ keV with supplemental beam heating of ≈23 MW during the burn phase will yield the best power performance. The $\overline{P}_E$ that can be obtained with $\alpha_{TIM} = 1$ in the beam-driven mode is comparable to the value that can be obtained with $\alpha_{TIM} = 15.2$ in the ignition mode, but $\overline{P}_{NET} < 0$ for the beam-driven mode. Larger values of $\overline{P}_E$ and $\overline{P}_{NET}$ would be

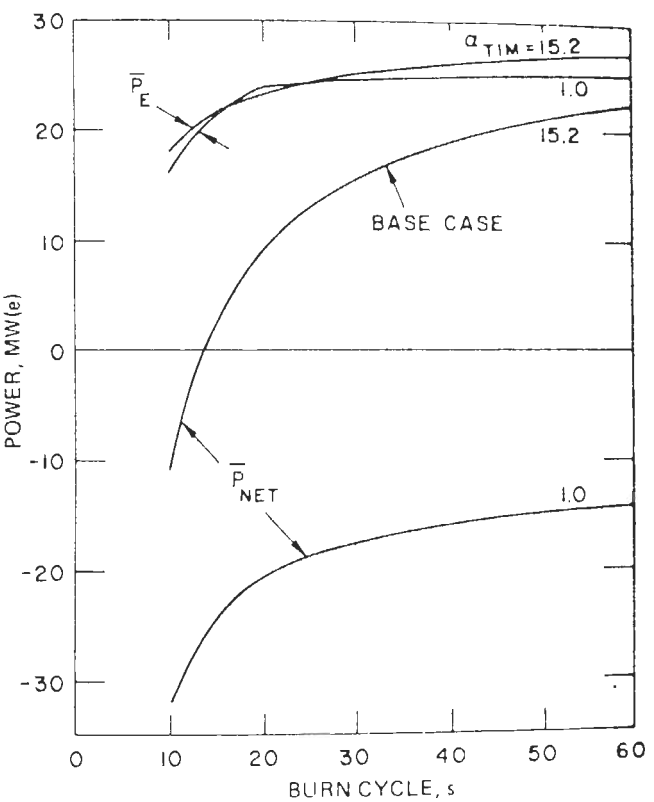

Fig. 10. Cycle-average electric power as a function of confinement.

obtained for $B_{max}^{TFC} > 70$ kG and for the noncircular design.

When wall-sputtered impurities are included in the analysis, the power performance may be substantially altered, depending on the wall material. For a low-Z wall coating, the power performance is only slightly degraded by wall-sputtered impurities. On the other hand, impurities sputtered from a stainless-steel wall would entirely preclude the possibility of $\overline{P}_{NET} > 0$ and would, for reasonable levels of supplemental beam heating during the burn phase, limit the burn-cycle duration to less than ≈20 s. With a silicon-carbide or aluminum wall, the power performance is degraded and the burn cycle is limited to less than ≈40 s, but $\overline{P}_{NET} > 0$ is possible.

The burn-cycle simulations were carried out under a variety of conditions to determine the requirements on the plasma heating and driving systems. For the circular plasma design:

1. the neutral-beam injection system must provide 40 MW of 180-keV beam power for 3 s
2. the plasma-driving system must provide ≈450 MJ of energy, with a peak power requirement of ≈1000 MW.

VI. MAGNET SYSTEM

The TEPR magnets analyzed in this design study consist of the TF, EF, and OH coils. The design approach taken here is a systems approach to design magnets that are an integral part of the system, rather than to develop an independent magnet design that does not fully take into account all the problems of a TEPR. The design of each magnet system is sufficiently developed so as to provide enough information about the main problems of each magnet system to indicate the necessary research and development program.

The proposed TF coils are fully stabilized superconducting magnets with NbTi as the superconductor and copper as the stabilizer. The TF coil shape has a pure-tension profile. The proposed EF and OH coils are fully stabilized ac fast-pulsed magnets with NbTi as the superconductor and cupronickel and copper as the stabilizer. Both EF and OH coils are located outside the TF coil system. The EF and OH copper coils are also studied. The I^2R loss for copper coils is much larger than for the superconducting coils. We conclude that a TEPR will have a better chance for breakeven, or net-power output, if both the EF and OH coils are superconducting. The main characteristics of the TF, EF, and OH coils are given in Fig. 11.

VI.A. TF Coil System

Because the power density is proportional to B_t^4, it is clear that the TF level must be as high as possible to minimize the TEPR size for a given power. The TF coils must be superconducting to achieve net power out. The NbTi is the best superconductor to use because of its ductility. The specification of a peak field of 75 kG (at 4.2 K) at the magnet winding is based on a practical judgment concerning some degree of margin required in a real system subjected to the superimposed rapidly pulsed field on the order of 5 kG from the EF and OH coils and the plasma current. Furthermore, the local temperature fluctuation during operation due to the pulsed field dissipation and the nuclear heating must be allowed for in the design.

One of the major problems with large TF coils is that of support. If the coil profile is circular, the nonuniform Lorentz forces will subject the TF coils to large bending stresses. Consequently, for a given coil structure, the coil reaches its stress limit before it reaches the peak field limit of NbTi. The minimum stress condition exists when the coil is in pure tension with no bending moments. We have developed a new analytical approach to determine a pure-tension coil profile, taking into account the number of coils, the coil cross section, and the gap size between two adjacent coils. The pure-tension computational model is described in Ref. 2. The three-dimensional stress analysis verified that our coils do indeed approach the pure-tension criterion with a peak stress of 20 000 psi and an average stress of 16 000 psi. For comparison, if the coils are circular, the peak stress will be 70 000 psi for the same inner and outer toroid dimensions (R_{10} and R_{20} in Fig. 11). If the coils have the so-called Princeton "simple D" shape,[13] the peak stress will be 60 000 psi.

The determination of the TF coil size was the result of an interactive process involving the plasma physics and power performance, the blanket and shield design, requirements for the OH coils, and the access requirements. For radiation protection, the thickness of the inner blanket and shield is 1 m. The inner radius (R_{10} in Fig. 11) was determined by the requirement that the central-core radius be sufficiently large so that the OH coil field need not be too high, and by the requirement that the plasma volume be sufficiently large to meet the power objective of the TEPR. For the design, the power objective can be satisfied by a circular plasma with a major radius, $R_0 = 6.25$ m, and minor radius, $a = 2.1$ m. The next dimensional requirement is the 3-m spacing between coils for neutral-beam injectors and for

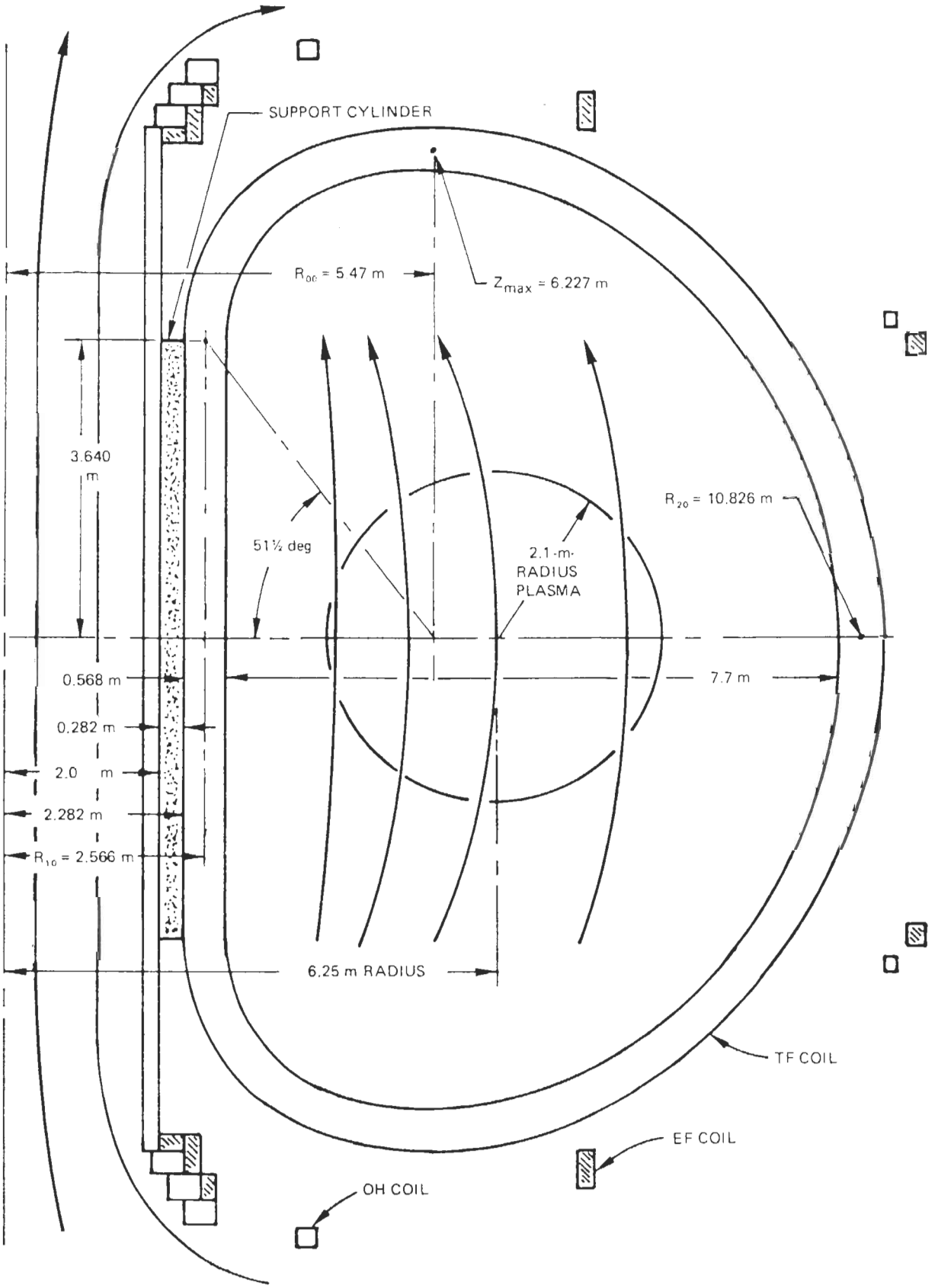

Fig. 11. Schematic of TEPR magnets design.

access for the installation and maintenance of the first wall, blanket, and shield. These requirements can be satisfied with 16 TF coils having an R_{bore} of 7.7 m and a maximum field ripple of 2%. The characteristics of the TF coils are given in Table XIV.

For a peak field of 75 kG, the average coil stress is 16 000 psi. A reasonable stress limit for the copper is ~12 000 psi. To maintain the stress level for copper with an average coil stress of 16 000 psi, the coil volume is roughly divided into one part copper, 0.5 part stainless steel, and 0.1 part coolant passage. The resulting stress in stainless steel is 24 000 psi.

Since the field decreases rapidly across the coil winding, the conductor will be made in three grades. Conductor design is based on the current-carrying capacity of NbTi at 4.2 K and peak fields of 76, 60, or 45 kG, depending on the grade of the conductor. The maximum radiation-induced resistivity in the copper is 2.5×10^{-8} Ω-cm for an integrated wall loading of 10 MW-yr/m^2. This induced resistivity decreases to 5×10^{-9} Ω-cm at the outer zone of the coil. The electrical insulation is Mylar, and the supporting material is stainless steel.

TABLE XIV

Superconducting Toroidal Field Coils

Superconductor/stabilizer/insulator/support	NbTi/copper/Mylar/stainless steel
Number of coils	16
Coil shape	Pure-tension D
Field ripple	2%
Maximum access	3.4 m
Operation temperature	4.2 K
Peak field due to TF coils	75 kG
Superimposed ac field	3 to 5 kG
Vertical bore	11.88 m
Horizontal bore	7.7 m
Field in plasma, B_t	34 kG
Operational current	10 000 A
Stored energy	975 MJ/coil, 15 600 MJ total
Inductance	19.5 H/coil, 312 H total
Ampere-turns	6.54×10^6/coil, 104.64×10^6 total
Turns per coil	654
Pancakes per coil	21
Mean turn length	34.4 m
Total conductor length	22 500 m/coil
Approximate weight	175 tons/coil, 2800 tons total
Coil and bobbin cross section	56.8 cm (radial) × 90 cm (axial)
Winding cross section	51.8 cm (radial) × 85 cm (axial)
Conductor width	3.6 cm
Conductor thickness	
inner zone	1.35 cm
central zone	1.217 cm
outer zone	1.0 cm
Stainless-steel thickness	
inner zone	0.6 cm
central zone	0.5 cm
outer zone	0.5 cm
Conductor current density	
inner zone (5 turns)	2459 A/cm^2
central zone (6 turns)	2572 A/cm^2
outer zone (20 turns)	3223 A/cm^2
Average current density	1280 A/cm^2 average over bobbin and coil
	1486 A/cm^2 average over coil winding
	2378 A/cm^2 overall average conductor

The basic coil unit will be a pancake module. The bobbin, having a pure-tension profile, is a stainless-steel casting, 2.5 cm thick all the way around. Each pancake will be wound directly on the bobbin. Between two pancake coils, a 0.4-cm-thick spacer is provided for force transmission and liquid-helium flow between the pancakes. Each pancake has 70% of both edges cooled. In addition, 50% cooling is provided on one face to fulfill the full-stabilization criterion. The stainless-steel support material will be distributed uniformly through the coil. This method of reinforcing provides the best stress distribution throughout the winding.

An ac field of ~3 kG will be superimposed on the TF coils by the OH coil, the EF coil, and the plasma. Assuming a 10-μm filament diameter for the conductor and a typical fusion cycle of 35 s during which the ac field makes a swing of $0 \rightarrow 3$ kG $\rightarrow 0$, the hysteresis loss per coil is 2700 J and the average power dissipation is 77 W/coil at 4.2 K. Assuming a reasonable short-twist pitch of 5 cm, no field shielding, and $\dot{B} = 3$ kG/s, the matrix loss per coil over a fusion cycle is 119 400 J or 3.411 kW/coil. However, if a field shield is used to slow down the flux-diffusion rate by a factor of 10, the matrix eddy-current loss will be 11 940 J/coil or 341 W/coil. To reduce the matrix loss further, the conductor could be made of a cable consisting of transposed multiple wires. Then the twist pitch could be reduced by a factor of 5, thus reducing the matrix loss by a factor of 25. The nuclear heating contributes 16 W/coil and the cryostat heat leak is ~13 W/coil. The total refrigeration requirement, with a field shield but without using transposed cable, is ~10 kW of refrigeration at 4.2 K.

The straight sections of the 16 TF coils exert a total centering force of 642×10^6 lb onto a central support cylinder having a 2-m inner radius and a 2.282-m outer radius. The cylinder is made of laminated stainless steel so that the eddy-current losses are reduced. The radial compression pressure is ~4000 psi; the maximum circumferential stress of the cylinder is 34 000 psi. Since the cylinder is at 4.2 K, this stress level poses no problem.

A series-connected coil protection scheme allows the stored energy to be rapidly dumped to a discharge resistor outside each TF coil to prevent damage under malfunction conditions. The series connection also ensures that each coil

carries equal current at all times so that no additional large forces are generated during a magnet quench.

VI.B. EF Coil System

The required equilibrium field for the TEPR is 3 kG. For stability against radial displacement, $|\partial B_{vz}/\partial R|$ must be <3.6 G/cm, where B_{vz} is the vertical field component and R is the toroidal radius. Note that $\partial B_{vz}/\partial R$ must always be negative. For stability against vertical displacement, the vertical-flux lines must be concave toward the toroidal axis.[14] The EF coils were carefully arranged so that the vertical field satisfies these plasma-stability requirements. Furthermore, they are arranged so that they are decoupled magnetically from the OH coil and yet produce a bonus of 37 V-s for the plasma, thus reducing the V-s requirement for the OH coils. After trying various EF coil locations, we found that if they are located external to the TF coil, the coil arrangement is very flexible, the assembly and disassembly are easier, and the pulsed field on the TF coil can be reduced. Further, since the EF coils are superconducting, their current-carrying ability is affected by the magnetic flux. Thus, if they were located inside the TF coils, they would require a high percentage of NbTi superconductor. Based on these requirements and considerations, the EF coil configuration shown in Fig. 11 was chosen. The magnet characteristics are tabulated in Table XV, and the vertical field pattern is indicated in Fig. 11.

The EF coil operational current is 15 000 A, with a charging time of 1 s and a field excursion of 0 → 37 kG. The fast pulsing suggests that the filaments must be small, twist-pitch must be short, and a three-component composite with a highly resistive barrier of cupronickel between filaments must be used. The high current and fine filaments suggest that the 15 000-A conductor cannot be made of one strand. Multiple-strand cable must be transposed to ensure good current sharing. Because of the large stored energy, the EF coil must be fully stabilized. This means that the strand diameter cannot be too large to ensure an adequate surface-to-volume ratio for cooling. With these considerations, and based on careful design calculations, the required composite diameter is found to be 0.6 mm, filament size is 5 μm, twist-pitch is 6 mm, and the number of composites in the cable is 243. Two cable schemes were examined and full stability was verified. The temperature rise and the amount of cooling during the field-swing process were estimated. For a complete fusion cycle of 35 s, the total hysteresis loss is 22 637 J, the total matrix loss is 4353 J, the total self-field loss is 224 J, and the ac pulsing loss of the equilibrium coil is 27 214 J. The average power dissipation is 777 W at 4.2 K or 233 kW at 300 K. In comparison, a water-cooled copper EF coil would have an average power dissipation of 92 MW.

TABLE XV

Superconducting Equilibrium Coils

Superconductor/stabilizer	NbTi/copper and cupronickel
Average current density	2300 A/cm^2
Equilibrium field	3.0 kG
Peak field	~37 kG
Ampere turns	10×10^6
Conductor length	727×10^3 A-m
Field rise in conductor	37 kG/s
Stored energy	900 MJ
Operational current	15 000 A
Inductance	0.8 H
Power supply voltage	37.7 kV
V-s to plasma	37 V-s
15 000-A Cable	
Composite diameter	0.6 mm
Composite operational current	61.7 A at 4.2 K
Composite critical current	2 × 61.7 A at 4.2 K
Composite composition	NbTi: copper: cupronickel = 0.23: 0.57: 0.2
Twist pitch	6 mm
Matrix resistivity	10^{-6} Ω-cm
Filament diameter	5 μm
Number of filaments in composite	3307
Number of composites in cable	243
Total composite volume	3.33 m^3
Total cable length	48 480 m

VI.C. OH Coil System

Based on the burn-cycle dynamics study, it appears that the required resistive V-s is less than the inductive V-s. Thus, the assumption that the required V-s is 2 $L_p I_p$ is conservative and one that should provide some margin. The L_p was computed to be 12.273 μH. With $I_p = 4.5 \times 10^6$ A, the total V-s is 110. (The I_p depends on the peak field and the safety factor, but 110 V-s is a representative requirement.) Since the EF coils supply 37 V-s, the required V-s for the OH coil is 73. The flux-core radius is 1.9 m, so the required central field is 32 kG, provided the coil is superconducting. The air-core transformer has the advantage of not requiring a massive iron core and, above all, leads to a smaller core-size requirement. The air-core superconducting transformer is chosen as the preferred design over the air-core water-cooled copper coil because it has a smaller power loss. The stored energy of the superconducting OH coil is around 890 MJ. Because of the large stored energy, the OH coil is designed to be fully stabilized.

The OH coils are located outside the TF coil system. The OH coil windings are so arranged that they impose a minimum field and torque on the TF coils. It is also necessary that the OH coil fields in the plasma-column region be nearly zero so that the plasma can be initially ionized. The winding configuration is shown in Fig. 11. The achieved minimum field in the plasma region is on the order of 10 G. The OH coils superimpose a field of 1 kG on the TF coil. The magnet characteristics are listed in Table XVI.

The OH coil current is 40 000 A, with a charging time of 1 s and a field excursion of -32 → +32 kG; therefore, $\dot{B}$ = 64 kG/s. The considerations in the design of the conductor composite and cables that applied to the EF coil apply as well to the OH coil. The required diameter for the composite is 0.5 mm. The conductor is a three-component composite with copper and cupronickel as the matrix.

The 40 000-A cable will have 729 strands, each carrying 54.9 A, with a 5-μm filament diameter and a 6-mm twist-pitch. The ac pulsing losses over a complete fusion cycle of 35 s are:

1. filament hysteresis loss—32 068 J
2. matrix loss—8800 J
3. self-field loss—500 J.

Thus, the total ac loss per cycle is 42 369 J and the average power dissipation is 1182 W at 4.2 K or 354 kW at 300 K. The cable is designed to be fully stable and the temperature rise for 64 kG/s is small, even with poor cooling. In comparison, a water-cooled copper OH coil would have an average power dissipation of 4.3 MW.

TABLE XVI

Superconducting OH Coils

Superconductor/stabilizer	NbTi/copper and cupronickel
Average current density	1280 A/cm^2
Central field	32 kG
Peak field	32 kG
Ampere turns	45×10^6
Conductor length	628×10^6 A-m
Stored energy	883 MJ
Field rise in conductor	64 kG/s
Operational current	40 000 A
Self inductance	1.1 H
Mutual inductance	958 μH
Power supply voltage	140 kV
V-s to plasma	73 V-s
40 000-A Cable	
Composite diameter	0.5 mm
Composite operational current	54.9 A at 4.2 K, 32 kG
Composite critical current	109.8 A
Composite composition	NbTi: copper: cupronickel = 0.26: 0.54: 0.20
Twist pitch	6 mm
Matrix resistivity	10^{-6} Ω-cm
Filament diameter	5 μm
Number of filaments in composite	2613
Number of composites in cable	729
Total composite volume	2.25 m^3
Total cable length	15 702 m

VII. PLASMA SUPPORT SYSTEMS

VII.A. Neutral Injection

Neutral deuteron-beam heating requirements for TEPR have been determined on the basis of burn-cycle dynamics calculations. Nominal neutral-beam requirements for the TEPR are given in Table VII.

The corresponding ion-source, beam-current, and power requirements have been determined for four different methods of producing the neutral beam. The most efficient method requires that D^- ions be extracted directly from a deuterium plasma and accelerated to the desired final energy before neutralization. This method, which requires the smallest ion-source currents, has been ruled out for the time being because a source suitable for even the present-day neutral-injection experiments does not presently exist. The second most efficient method, but the one that demands the largest ion-source currents, requires that positive ions (D^+, D_2^+, D_3^+) extracted from a deuterium plasma be converted, at low energy (several keV) into D^- ions, which are then accelerated to the required neutral-beam energy before injection into a neutralizer cell. This method has been ruled out for the TEPR not only because a suitable charge-exchange source does not presently exist but, also, because of the very high positive-ion currents that are needed. The least efficient methods require that positive ions be extracted from a deuterium plasma and accelerated to the required energy before injection into the neutralizer. In one scheme, the ions are accelerated to full energy before optional removal of the molecular components of the ion beam. If the option is exercised, the D^+ beam is then neutralized; if not, all three components of the ion beam are neutralized. This method, with all the ion-beam components neutralized, is the one presently used for neutral injection into controlled thermonuclear reactor (CTR) devices. We have chosen this method, with optional removal of unwanted molecular ion-beam components and energy recovery, for the reference design.

An ion-beam energy of 180 keV was chosen on the basis of plasma penetration considerations. An energy capture efficiency of 95% was estimated for the TEPR plasma density and dimensions,

taking into account the intersection of fast deuteron-ion orbits with the vacuum wall.

For the neutral-beam production model of Fig. 12, the neutral injection efficiency is plotted in Fig. 13 as a function of the ion-beam voltage for one- and three-component neutral beams, with and without energy recovery.

To obtain tens of amperes of ion beam from a single source, it is necessary to have large-area extraction systems, and this has led to the use in CTR sources of large multiaperture, or multislot, extraction grids. The total amount of extraction-electrode grid area required to produce a given amount of neutral-beam power is shown in Fig. 14 for an extracted-current density (total extracted current/total extraction grid area) of 125 mA/cm^2; curves are drawn for several beam voltages for one- and three-component neutral beams, with and without energy recovery.

At the present time, Berkeley[15] and Oak Ridge[16] ion sources are in the forefront of the advance toward the type of source required for TEPR, although the power efficiencies of these types of source at 180 keV are rather low. Thus, they, along with relatively well-established vacuum, power, and beam-handling (deflecting, focusing) technologies, form the technological basis for the neutral-injector designs. The TEPR design requires significant extrapolations beyond the present state-of-the-art.

VII.B. Vacuum Systems

There will be two vacuum systems associated with the operation of the TEPR: the toroidal vacuum system and the neutral-beam vacuum system (see Table VIII). These two systems are interdependent to some extent, since beam injection is through ports in the toroidal vacuum vessel. Both systems will be served by a common secondary pumping system for pumping down from atmosphere to operating pressure of the primary pumps. This same secondary system can be used for bake-out cycles, for holding pumps, and as a backup system for regeneration of the cryosorption pumps.

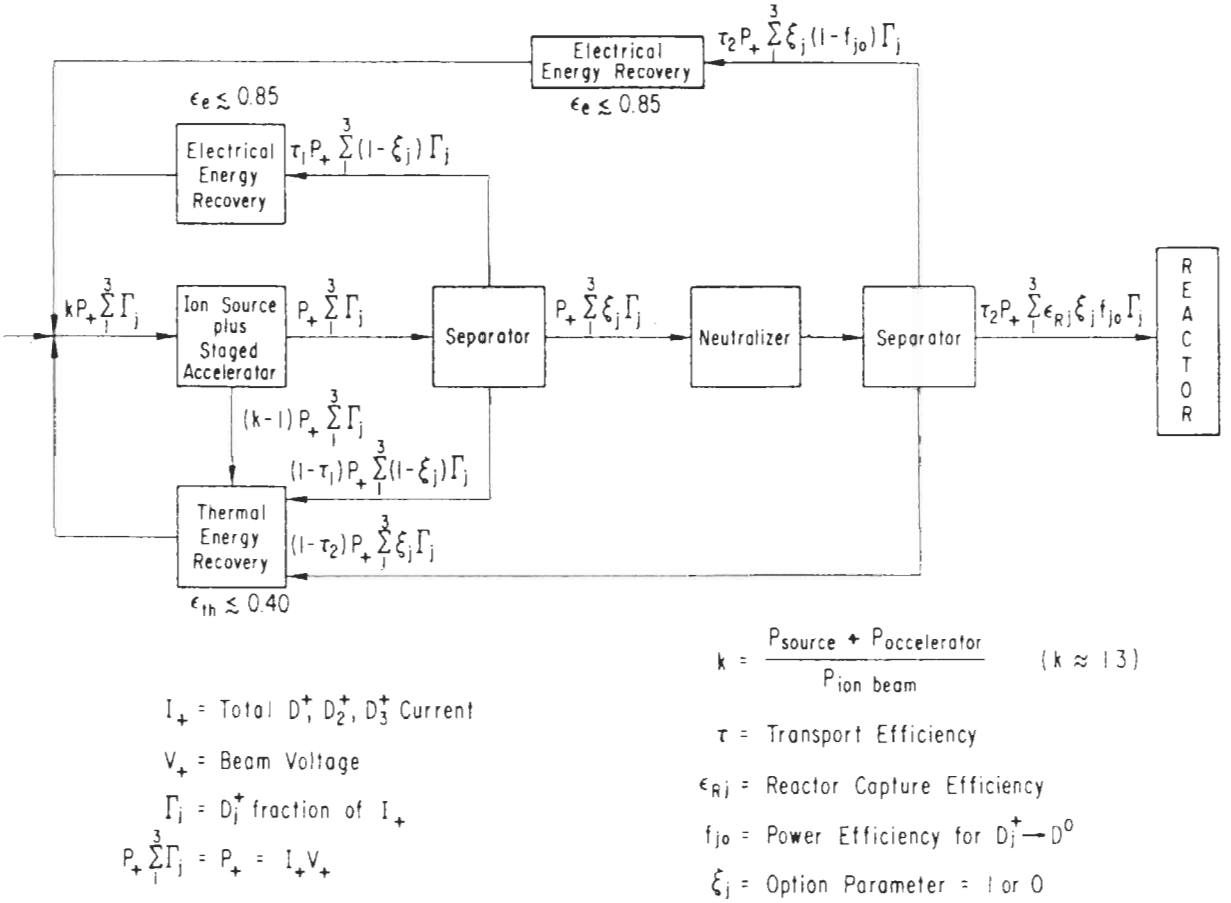

Fig. 12. ANL neutral-beam production model for $D_j^+ \rightarrow D^0$, $j = 1, 2, 3$, with the ion beam accelerated to full energy before optional removal of molecular components.

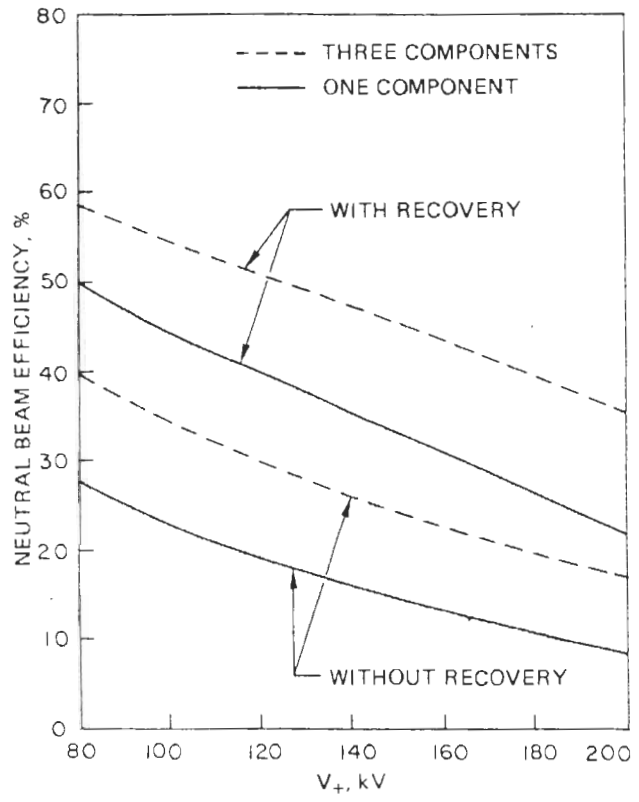

Fig. 13. Neutral-beam production efficiency versus ion-beam voltage for the model of Fig. 12 with $\Gamma_1 = 0.75$, $\Gamma_2 = 0.18$, $\Gamma_3 = 0.007$, $\tau_2 = 0.8$, and $\epsilon_{Rj} = 0.95$, $j = 1, 2, 3$ ($\tau_1 = 1.0$).

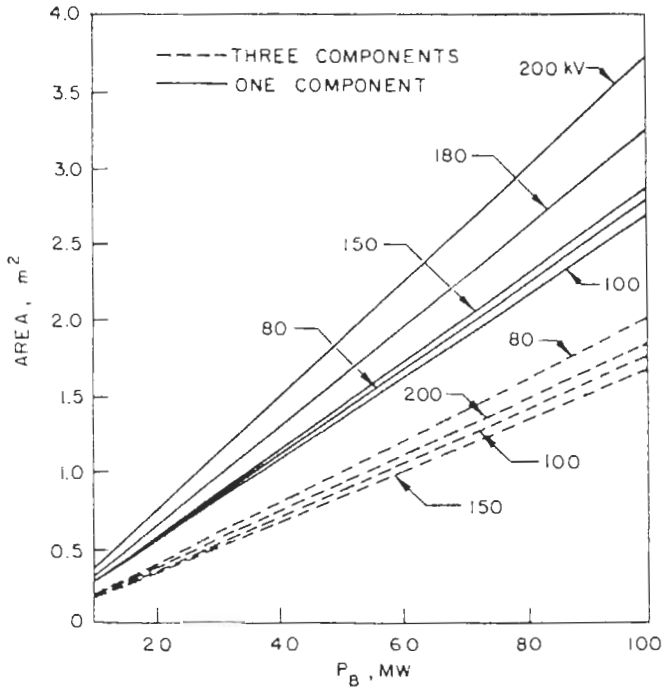

Fig. 14. Extraction grid area versus neutral-beam power for an extracted current density of 125 mA/cm² ($D_j^+ \rightarrow D^0$).

The primary pumps being considered for reaching and maintaining operating pressure in the toroidal vacuum system are cryosorption pumps. These pumps are being considered because they reduce the space problem that diffusion pumps present and the more difficult tritium recovery and maintenance necessary with ion pumps and sublimation pumps. They have the ability to generate an inherently "clean" vacuum, which is not contaminated by oil vapors or other impurities, and operation is not immediately affected by power failures. Moreover, cryosorption pumps can vary in configuration so that they may be attached to vacuum systems at almost any point. Special pumps can quite easily be constructed by simple scale-up to almost any imaginable size to achieve desired pumping speeds and mass throughput rates. The neutral-beam injector vacuum system will require large-area cryosorption panels.

Although cryosorption pumps are a conventional form of pumping, they can be classified here as developmental because of the unavailability, at present, of pumps with the speeds required and the added feature of a closed vacuum system due to the presence of tritium. Even the secondary pumping system must be classified as developmental because of the limited selection of so-called "canned" pumps, which eliminate exposure of seals and thus the possibility of tritium leakage into the atmosphere.

VII.C. Power Supplies

The current in the OH coil reverses twice each reactor cycle, causing the total stored energy of the magnet to be transferred into and out of the OH coil power supply twice a cycle. Since the energy of the coil is $\sim 10^9$ J, the energy storage and transfer portion of the OH coil power supply is the dominant feature of the design. The maximum voltage and current that must be handled during the cycle is 140 000 V and 40 000 A. Conventional energy storage systems, such as capacitors and motor-generator-flywheel sets, will be too costly and/or inefficient. Homopolar generators[17] or superconducting magnetic-energy transfer systems[18] might be applicable, but research and development are required.

An arrangement of concentrically stacked drum-type homopolar generators is being studied for this application. The basic geometry is shown in Fig. 15. Thin shell conducting cylinders of different diameters are aligned around the generator center line. Insulating cylinders are placed between each conducting cylinder. The insulating cylinders are supported from the center shaft by spokes at the edges. The conducting cylinders are free to rotate. Brushes are located at the edges

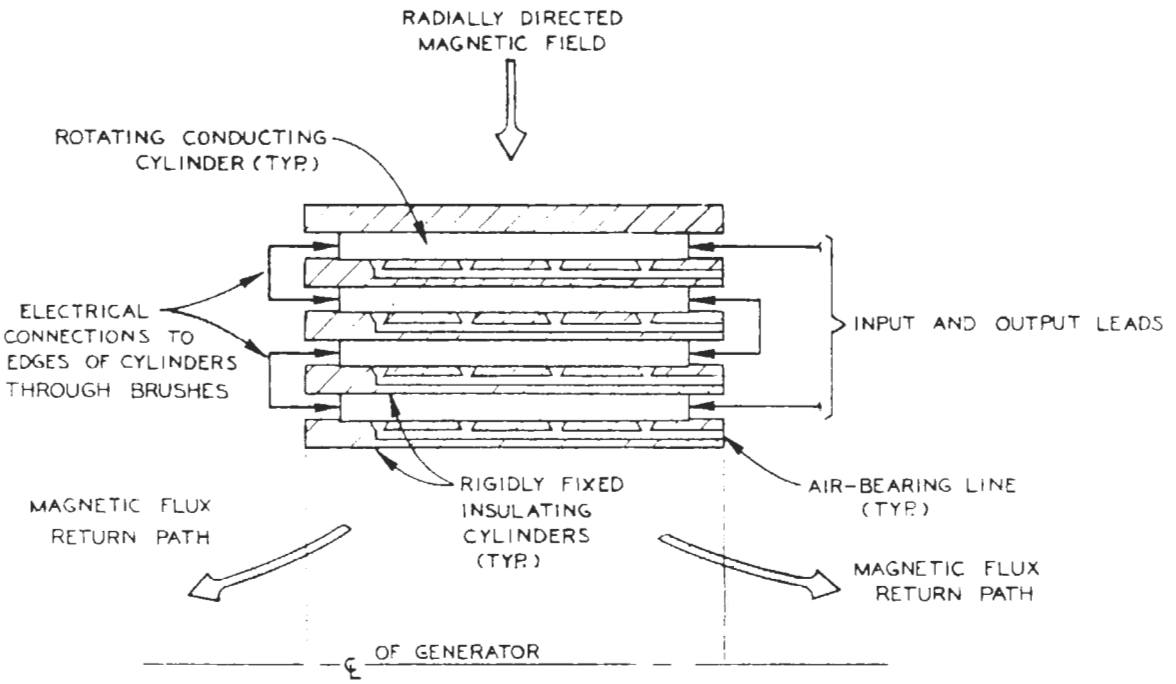

Fig. 15. Cross section of the region of insulating cylinders and conducting drums for a typical CCG.

of the conducting cylinders and are connected so that adjacent cylinders will counter-rotate in the presence of a radially directed magnetic field. The conducting drums are supported on air bearings that allow them to rotate in either direction. The innermost and outermost cylinders are made of insulating material so that electrical insulation between ground and conducting cylinders can be supported to high-voltage levels. We call this homopolar arrangement the Counter Cyclonic Generator (CCG).

Superconducting coils operating at ~7.5 T and 4000 A/cm^2 are under consideration. The magnetic yoke arrangement is shown in Fig. 16. The iron operates in a highly saturated state, but still provides about a factor of 2 in ampere turns and a much better field distribution in the drum region. Whether or not these benefits are offset by higher unit cost has not yet been studied.

The parameters for a typical CCG 100 000-A module currently under investigation are given in Table XVII. The conducting drums are constructed of Type 17-4 stainless-steel cylinders, 0.9 m long. The radial gap extends from 0.9 to 1.32 m. Eight stainless-steel drums of varying radial thicknesses are stacked in this gap, supported by insulating drums of 0.035-m-thick stainless-steel-reinforced epoxy fiberglass. Each cylinder thickness is adjusted to grade the voltage across the generator so that each cylinder operates at a peak surface velocity of 236 m/s. This leads to a stress that is ~85% of the elastic yield point. The CCG modules would be connected in series to match the coil impedance.

The CCG arrangement looks attractive from a cost and efficiency standpoint, but further studies on technical problems and cost optimization are required.

The power supply for the EF coil also requires an energy transfer unit that is basically similar to the OH coil, except that the energy must be stored in the power supply for the duration of the exhaust and replenishment phase of the burn cycle.

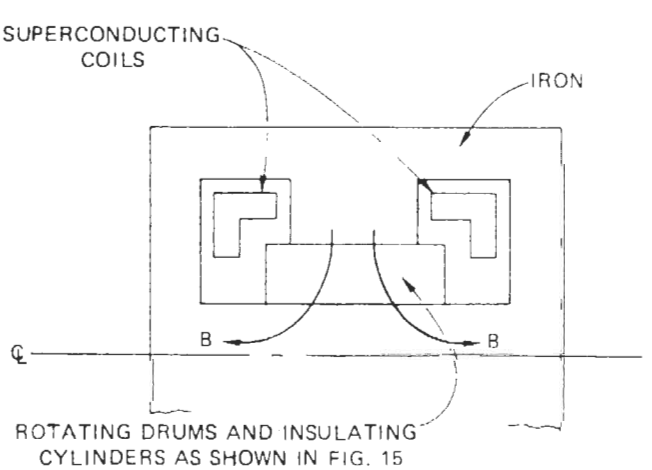

Fig. 16. Cross section of reference design for a CCG module.

TABLE XVII

Parameters for a CCG Module Using 0.9-m-long Type 17-4 Stainless-Steel Drums with a 236 m/s Surface Velocity

Cylinder Number	Inner Radius (m)	Radial Thickness (m)	Induced Voltage (V)	Effective Capacitance (F)	Stored Energy (MJ)
1	0.9250	0.0152	1086	29.3	17.3
2	0.9773	0.0147	1104	28.8	17.6
3	1.0291	0.0140	1114	28.6	17.7
4	1.0802	0.0135	1123	28.3	17.8
5	1.1308	0.0131	1140	27.9	18.1
6	1.1810	0.0126	1152	27.6	18.3
7	1.2307	0.0123	1168	27.3	18.6
8	1.2801	0.0120	1180	27.0	18.8
Total CCG Module			9067	3.511	144.3

The present TEPR design requires 40 MW of 180-keV neutral beam. At an efficiency of 50%, the neutral-beam power supply must deliver 80 MW at 180 kV for a duration of 3 s. A polyphase phase-controlled rectifier system is probably the most straightforward way to generate that much power at 180 kV. Emergency phaseback will be employed to prevent excessive damage to the accelerating column during sparking in the event of switchtube failure. Also, to prevent loading the power grid, a motor-generator-flywheel set will be used to distribute the power demand.

VIII. PRIMARY ENERGY CONVERSION SYSTEM (PECS)

For the purpose of this paper, all of the components and hardware that lie between the plasma and TF coils have been considered collectively under PECS. Included in this system are:

1. the first wall
2. the blanket (~99% of the neutron and gamma radiation is converted to sensible heat in these two regions)
3. the primary coolant, which removes sensible heat from the blanket
4. the shield, which backs up the blanket region and provides the additional neutron and gamma attenuation required to protect the TF coils
5. all the penetrations into and/or through the blanket/shield region that provide access for neutral-beam injection, evacuation, coolant inlet, and removal, diagnostics, maintenance, experimentation, etc.

The preliminary PECS design for the Stage I and Stage II TEPR, together with results of the materials assessments and parameter analyses that supported the design activity, are summarized in this section.

VIII.A. Stage I PECS

The Stage I PECS is designed to:

1. permit the generation and removal of ~100 MW of sensible heat
2. provide adequate protection of the magnet system from radiation damage and activation and excessive nuclear-energy deposition
3. allow continuous operation of reactor-level plasmas at a plant duty factor of ~30%
4. demonstrate all operational aspects of a Tokamak fusion power reactor except tritium breeding and breeder-blanket performance.

Materials and design approaches for the Stage I PECS were selected on the basis that they:

1. satisfy the nuclear requirements for nuclear-energy production and radiation attenuation
2. permit PECS construction, operation, and maintenance with minimum advancement in existing technology
3. provide a reasonable point for extrapolation to a demonstration-scale Tokamak fusion power reactor.

VIII.A.1. First-Wall Design Considerations

The first wall (treated as a subsystem of the PECS) includes the vacuum vessel that surrounds the plasma region and other associated components; i.e., a low-Z coating, a plasma-aperture

limiter, a flux breaker, and the vacuum wall penetrations. The principal requirements of the TEPR first wall are:

1. to protect the plasma region from excessive atmospheric contamination
2. to prevent excessive plasma contamination by products of plasma-wall interactions
3. to maintain its structural integrity for sufficient times under the severe irradiation, thermal, and stress conditions imposed by an operating fusion reactor environment.

The first-wall system design options that have been considered for the TEPR include:

1. a bare-metal first wall
2. a first wall fabricated from sintered metal-metal oxide product of the sintered aluminum product (SAP) type
3. a composite consisting of a metal vacuum wall with a protective low-Z coating
4. a metal vacuum wall protected from the plasma by a separate low-Z liner.

The bare-metal wall is the most attractive of the four options on the basis of fabricability, but the relatively high-atomic number (high-Z) of the atoms sputtered from typical structural metal surfaces (e.g., stainless steel, vanadium-base alloys) prevents the attainment of reasonable plasma ignition and burn conditions. The latter three first-wall options are aimed at use of a low-Z material as the first surface facing the plasma. The SAP-type materials are considered to be of marginal utility because of their relatively low melting point and questionable radiation damage characteristics. For the design effort described in this paper, emphasis was placed on the use of a low-Z material, either as a coating on the vacuum vessel inside wall or as a separate, radiatively cooled liner. The coating option has several attractive features with respect to utilization in the TEPR; the major one appears to be of much simpler fabrication. It is conceivable that the coating could be put on after the vacuum wall is assembled, and replaced remotely after extended reactor operation. Drawbacks to the implementation of a radiatively cooled liner stem from the high operating temperature of the liner ($>1500°C$), the possibility of establishing a discharge in the annulus between the liner and the vacuum vessel, and the additional vacuum pumping requirements. Also, remote replacement for the separate-liner option appears to be less easily accomplished than for the coated wall option.

The preliminary first-wall design that has evolved for the Stage I PECS consists of stainless-steel panels coated with a thin (~ 100-μm) layer of a low-Z material (beryllium, BeO, B_4C, SiC, or carbon) on the inside to provide an interface between the plasma and the first-structural surface facing it that will permit ignition without continuous impurity removal. Several of the stainless-steel sections are fitted with brazed, insulated joints that are intended to disrupt the current that would otherwise develop in the first wall when the OH coils are pulsed. Additional details of the first-wall mechanical and structural design are given in Sec. VIII.C.

VIII.A.2. Blanket/Shield Design Considerations

The blanket region for the TEPR described in this paper has been designed to convert the neutron and secondary gamma-ray kinetic energies to sensible heat. Other important functions of the combined blanket/shield region are:

1. to reduce radiation damage in the TF coils to acceptable levels from the standpoint of induced stabilizer resistivity, decreased critical current, and superinsulation deterioration
2. to reduce nuclear heating in the TF coil system to tolerable levels
3. to minimize the induced activation and biological dose in the magnet structure.

All of these functions have to be performed with materials that:

1. are mutually compatible
2. can withstand radiation damage for reasonable operating lifetimes
3. can be fabricated and/or implemented with existing or near-term technology.

The radiation-induced resistivity in the copper stabilizer of the TF coil system should not exceed 2.5×10^{-8} Ω-cm, which corresponds to 1.87×10^{-4} dpa, from the standpoint of magnet economics and reliability. This resistivity results from atomic displacement damage caused by the neutrons and can be annealed out by warming the magnet to near room temperature. Since the magnet cooldown could take as much as two months, the blanket/shield region should be designed to permit reactor operation at reasonable plant-duty factors (up to 50%) and wall loadings (≈ 0.2 MW/m^2) for sufficiently long time spans between anneals (≥ 2 yr). Nuclear heating of the TF coils must be reduced to the point at which the refrigeration power requirements are on the order of 1% of the reactor power output. In addition,

there is incentive to minimize the blanket plus shield thickness on the inside of the torus so as to maximize the magnetic field in the plasma.

Nuclear performance characteristics of a variety of plausible materials compositions, which might meet the design requirements for the TEPR blanket/shield region, have been investigated. Some materials and compositions that have been considered are summarized in Table XVIII. Options employing stainless steel were chosen because of the excellent radiation-attenuating characteristics of stainless steel and because it is a construction material for which a substantial technology base exists. Options employing tungsten and tantalum were considered on the basis of their being superior to stainless steel in attenuating neutron and gamma radiation. Vanadium was considered because of the favorable compatibility of vanadium-base alloys with liquid lithium and because of its reasonably good nuclear performance characteristics. Options containing graphite and aluminum were investigated because they lend themselves to the development of a minimum activation blanket/shield assembly for a TEPR. Figure 17 shows the relationship between displacement damage in the magnet stabilizer and overall blanket/shield thickness for the various materials compositions investigated. Results of a similar sensitivity study, wherein the refrigeration power (as a percentage of the plant electrical power output) needed to overcome the nuclear heat load generated in the TF coil is plotted against overall blanket/shield thickness in Fig. 18.

Implications of the results in Figs. 17 and 18 and of other related parameter sensitivity analyses performed on the compositions given in Table XVIII may be summarized as follows:

1. Mixtures of stainless steel and boron carbide (B_4C) were found to be superior to all material compositions investigated, except for mixtures of tungsten (or tantalum) and B_4C, from the standpoint of reduced stabilizer displacement damage and nuclear energy deposition in the magnet. (The composition 50% stainless steel–50% B_4C was found to be optimal for reducing displacement damage to the stabilizer, while the composition 75% stainless steel–25% B_4C was optimal for minimizing nuclear energy deposition in the magnet.)

2. Studies of the induced radioactivity generated in the blanket/shield, after representative operating times, indicate that remote handling and

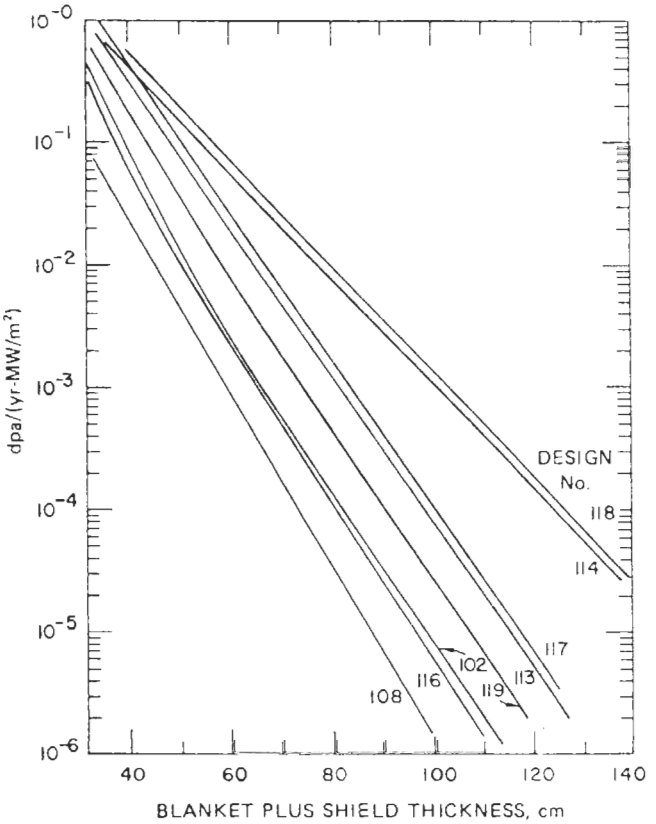

Fig. 17. Displacement damage to the superconductor stabilizer (copper) versus overall blanket/shield thickness for the materials compositions given in Table XVIII.

TABLE XVIII

Material Composition Options Considered for the TEPR Blanket/Shield Region

Design Number	Blanket (30 cm thick)	Magnet Shield (variable thickness)
102	30-cm stainless steel	50% stainless steel + 50% B_4C
108	30-cm 50% tungsten + 50% B_4C	50% tungsten + 50% B_4C
113	30-cm aluminum	50% stainless steel + 50% B_4C
114	30-cm aluminum	50% aluminum + 50% B_4C
116	30-cm stainless steel	75% stainless steel + 20% H_2O + 5% boron
117	30-cm graphite	50% stainless steel + 50% B_4C
118	30-cm graphite	50% aluminum + 50% B_4C
119	30-cm vanadium	50% stainless steel + 50% B_4C

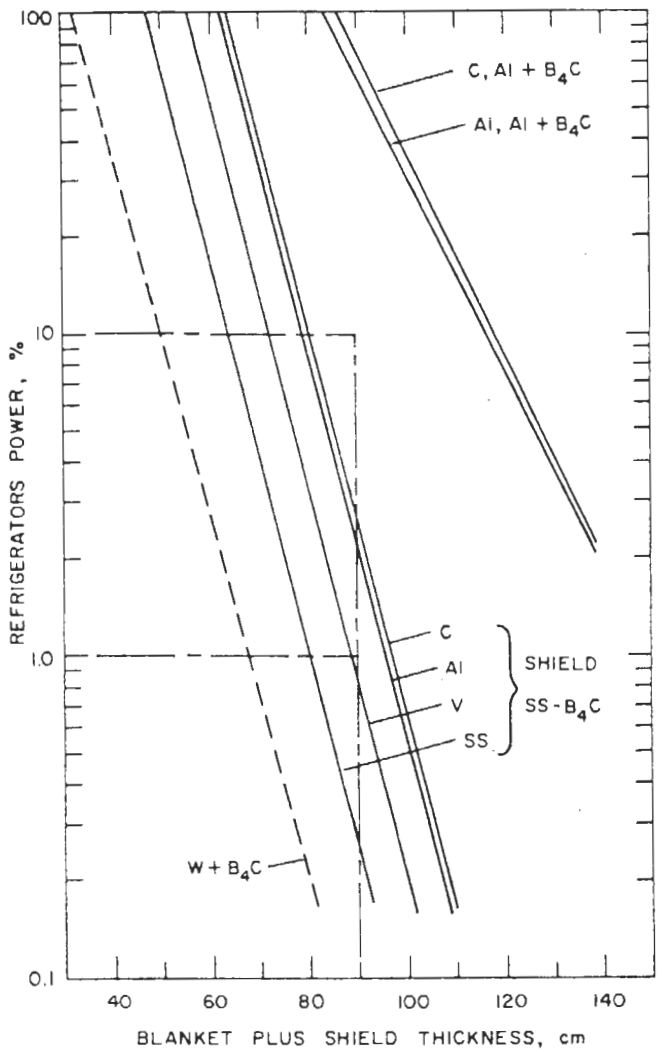

Fig. 18. Refrigeration power requirements (in percent of plant electric power output) versus overall blanket/shield thickness for the materials compositions given in Table XVIII (assumed thermal-to-electrical conversion efficiency = 30%).

maintenance would be required for the options employing stainless steel, tungsten (or tantalum), or vanadium even after a year of cooldown, whereas graphite and/or aluminum-containing compositions appear to be accessible (after only a few weeks cooldown) with a minimal degree of radiation protection.

3. Designs employing tungsten (or tantalum)-B_4C and stainless-steel-B_4C mixtures offer the best prospects for achieving magnet-protection objective with the smallest blanket/shield thickness (viz., Fig. 17).

4. The tungsten (or tantalum)-B_4C and stainless-steel-B_4C designs offer the best prospects for operation with small additional refrigeration power requirements due to nuclear heat deposition in the magnets (viz., Fig. 18).

5. Compositions that offer the best prospects for minimal remote maintenance (e.g., compositions employing only graphite and/or aluminum together with B_4C) appear to be incapable of leading to a blanket/shield design with overall thickness <1 m that would protect the magnets.

In light of the above results, the materials option employing optimized compositions of stainless steel and B_4C was selected for the preliminary blanket/shield design for the TEPR. An alternative design for the interior blanket/shield region, which consisted of an optimized composition of tungsten and B_4C, was carried along in parallel with the stainless-steel-B_4C design in the event that:

1. Additional radiation attenuation, over and above that provided by the stainless-steel-B_4C mixture, would eventually be required.
2. A sufficiently strong incentive arose to reduce the overall blanket/shield thickness to an absolute minimum value to increase the thermal power output.

Dependence of the blanket/shield thickness that limits the radiation-induced resistivity in the stabilizer to 3×10^{-8} Ω-cm on neutron wall loading, time span between magnet anneals and plant-duty cycle are given in Table XIX for the stainless-steel-B_4C preliminary design composition. Corresponding refrigeration powers are also given. Cases 6, 7, 11, and 12 are considered to represent reasonable operating conditions for the Stage I TEPR. For cases where the refrigeration power exceeds 10% of the plant electrical power output, it would probably be necessary to increase the blanket/shield thickness to bring the refrigeration power loading down to an economically more tenable level.

The optimized material disposition for the stainless-steel-B_4C reference TEPR interior blanket/shield region versus radial distance from the center of the plasma is given as Design I in Table XX. Material dispositions for three alternative designs are also given. Design II is the same as Design I except that the stainless steel in several interior zones is replaced by tungsten to enhance the total radiation attenuation. Designs III and IV represent optimized material dispositions for tungsten-B_4C and tantalum-B_4C mixtures. Stainless steel was included to a certain extent in Designs II, III, and IV to accommodate structural requirements. Table XXI contains a summary of important radiation damage parameters for the four designs given in Table XX.

TABLE XIX

Dependence of Blanket Plus Shield Thickness and Refrigerator-Power Requirements on Integral Wall Loading if the Maximum Allowable Radiation-Induced Resistivity in the Stabilizing Copper Conductor is 3×10^{-8} Ω-cm

Case	Neutron-Wall Loading (MW/m^2)	Span Between Magnet Anneals (yr)	Duty Factor (%)	Integral Wall Loading ($MW-yr/m^2$)	Blanket Plus Shield Thickness[a] (cm)	Refrigerator Power[b] (%)
1	0.1	2	20	0.04	59	113
2	0.1	2	50	0.10	67	33
3	0.1	2	80	0.16	71.5	18
4	0.1	5	80	0.40	77	9
5	0.1	20	80	1.60	87.5	1.5
6	0.2	2	20	0.08	65	3.3
7	0.2	2	50	0.20	72.5	16
8	0.2	2	80	0.32	75.5	11
9	0.2	5	80	0.8	81	6
10	0.2	20	80	3.2	92.5	1
11	0.5	2	20	0.20	72.5	16
12	0.5	2	50	0.50	78.5	7.5
13	0.5	2	80	0.80	81.0	6
14	0.5	5	80	2.0	89	1.4
15	0.5	20	80	8.0	97	0.6
16	1.0	5	80	4.0	93.5	1
17	1.0	20	80	16.0	107	0.15

[a]Based on optimized blanket and shield composition of stainless steel and boron carbide; the calculations allowed a void fraction (for helium cooling, thermal expansion, etc.) of 10 vol% in the first 40 cm, and 5% in the rest of the shield.

[b]Refrigeration electric-power requirements expressed in percentage of plant electric-power output. Assumptions: 70% of the outer surface area covered by the magnet, plant thermal efficiency of 30%, 16.5 MeV are recoverable for each fusion reaction, and 500-W electric power required per watt of thermal-power input to the refrigerators.

TABLE XX

Description of Alternative Designs for the Inner Blanket/Shield System

Zone	Radial Position (cm)	Thickness (cm)	Density Factor	Design I[a]	Design II	Design III	Design IV
1	0-210	210	0	Plasma	Plasma	Plasma	Plasma
2	210-240	30	0	Vacuum	Vacuum	Vacuum	Vacuum
3	240-241	1	0.5	Stainless Steel	Stainless Steel	Stainless Steel	Stainless Steel
4	241-256	15	0.9	Stainless Steel	Tungsten	Tungsten	Tantalum
5	256-261	5	0.9	B_4C	B_4C	Tungsten	Tantalum
6	261-276	15	0.9	Stainless Steel	Tungsten	Tungsten	Tantalum
7	276-281	5	0.9	B_4C	B_4C	B_4C	B_4C
8	281-291	10	0.95	Stainless Steel	Stainless Steel	Stainless Steel	Stainless Steel
9	291-301	10	0.95	B_4C	B_4C	Tungsten	Tantalum
10	301-311	10	0.95	Stainless Steel	Tungsten	Tungsten	Tantalum
11	311-321	10	0.95	B_4C	B_4C	Tungsten	Tantalum
12	321-331	10	0.95	Stainless Steel	Stainless Steel	Stainless Steel	Stainless Steel
13	331-340	9	0.95	B_4C	B_4C	B_4C	B_4C
14	340-397	57	1	magnet (44% stainless steel + 44% copper + 6% NbTi + 6% helium)			

[a]Reference design.

TABLE XXI

Radiation Damage Parameters in the TEPR TF Magnet for Designs Described in Table XX

Maximum Values in the Inner Magnet	Design I[a]	Design II	Design III	Design IV
Displacements in copper, dpa per MW-yr/m^2	1.5×10^{-5}	3.0×10^{-6}	1.4×10^{-6}	2.3×10^{-6}
Radiation-induced resistivity in copper, Ω-cm per 10 MW-yr/m^2	2.5×10^{-8}	5.0×10^{-9}	2.4×10^{-9}	3.9×10^{-9}
Neutron fluence, n/cm^2 per MW-yr/m^2	4.7×10^{16}	9.3×10^{15}	1.2×10^{16}	1.5×10^{16}
Dose in Mylar, rad per MW-yr/m^2	3.7×10^{7}	7.4×10^{6}	4.0×10^{6}	6.2×10^{6}

[a]Reference design.

VIII.A.3. Thermal Fluid Analysis for the Preliminary PECS Design

Both pressurized helium and pressurized water were considered for the primary blanket coolant in the reference PECS design. Preliminary thermal fluid analyses for the blanket configuration given as Design I in Table XX are summarized in Table XXII. For the same cooling configuration, blanket temperature profile, total thermal power, and thermal power deposition profile (determined from the nuclear heating calculations), pressurized water is found to require significantly less pumping power and coolant-channel volume fraction.

TABLE XXII

Thermal Fluid Analysis Parameters for the TEPR Preliminary Blanket Design

Parameter	Coolant	
	Water[a]	Helium[b]
Thermal power removed,[c] MW	186[d]	186[d]
Coolant inlet pressure,[c] atm	136	50
Pressure drop in blanket,[e] atm	<1	~1
Coolant channel diameter,[c] cm	1.0	2.5
Coolant channel volume fraction in blanket,[f] 1%	1→0.1	10→2
Pumping power for blanket, MW	<1	~7
Coolant inlet temperature,[c] °C	38	357
Coolant exit temperature,[c] °C	302	527
Maximum blanket temperature,[c] °C	600	600
Tube wall temperature,[c] °C	327	550
Number of radial zones[c]	6	6
Coolant velocity	[g]	[g]

[a]Parameters consistent with PWR technology.
[b]Parameters consistent with HTGR technology.
[c]Parameters fixed in calculations.
[d]Based on a conservative overestimate of the neutron wall load of 0.3 MW/m^2.
[e]Average pressure drop per tube.
[f]Required volume fraction for coolant decreases with radial distance from first wall.
[g]Incompressible flow was assumed, i.e., the coolant velocity was kept at $<0.3 \times$ sonic velocity.

It should be noted that:

1. The two alternative coolant schemes were not optimized with respect to electrical power output per unit of thermonuclear power.
2. The coolant-channel geometry was not optimized.
3. The stresses resulting from the indicated temperature profile remain to be analyzed.

While helium appears to have greater long-range potential as a fusion reactor coolant, the advantages of reduced coolant-channel volume fraction and lower pumping power afforded by water could help to ameliorate several of the design complications for the Stage I PECS.

The shield region, which backs up the blanket, is simply an extension of the blanket insofar as materials composition is concerned, but is operated at or near ambient temperature and is cooled with a low-temperature coolant circuit (probably borated water) that is separate and distinct from the primary coolant circuit. The substitution of tantalum or tungsten for the stainless-steel zones in the blanket and shield will require that the respective coolants be channeled through stainless-steel ductwork or that the tantalum (or tungsten) be canned in stainless steel to avoid materials incompatibilities between helium or water and the refractory metals.

VIII.B. Stage II PECS

The criteria for the Stage II PECS module designs are largely the same as those for the Stage I design, except that appropriate modifications are required to include a tritium-breeding medium. These modifications consist of introducing a relatively thin zone (~10 cm) of liquid lithium or a solid lithium compound. In the liquid lithium design, the blanket structure would be altered to include the use of a vanadium-base alloy for lithium containment. The solid lithium

compound would be selected to be compatible with stainless steel and would be operated in a packed-bed mode. If MHD effects on heat transfer and pressure drop, resulting from the circulation of a liquid metal in Tokamak-type magnetic-field environments, prove to be tolerable, consideration will be given to the use of liquid lithium as primary coolant in a Stage II blanket module. Otherwise, both the liquid-lithium and solid-lithium compound blankets could be cooled with pressurized helium, although thermal energy removal and materials compatibility problems are expected to be exacerbated in this case.

Consideration was given to the demonstration of net breeding gain for the Stage II modules. (The breeding gain with a Stage II module would be sufficient to achieve net breeding if the entire blanket were so constructed.) The overall thickness of the Stage II PECS modules must not exceed a value that is compatible with the basic Stage I design. The relationship between displacement damage to the TF coil stabilizer and overall blanket/shield thickness for three plausible breeding configurations is given in Fig. 19, together with the curve for an all stainless-steel blanket for comparison purposes. The results in Fig. 19 show that a net breeding gain is possible with a relatively thin zone (~10 cm) of enriched lithium (~90% ^{6}Li) and beryllium. A demonstrated breeding gain in a zone of thickness ≤10 cm does not appear to be possible for designs that employ enriched lithium (without any beryllium) or natural lithium (~92% ^{7}Li).

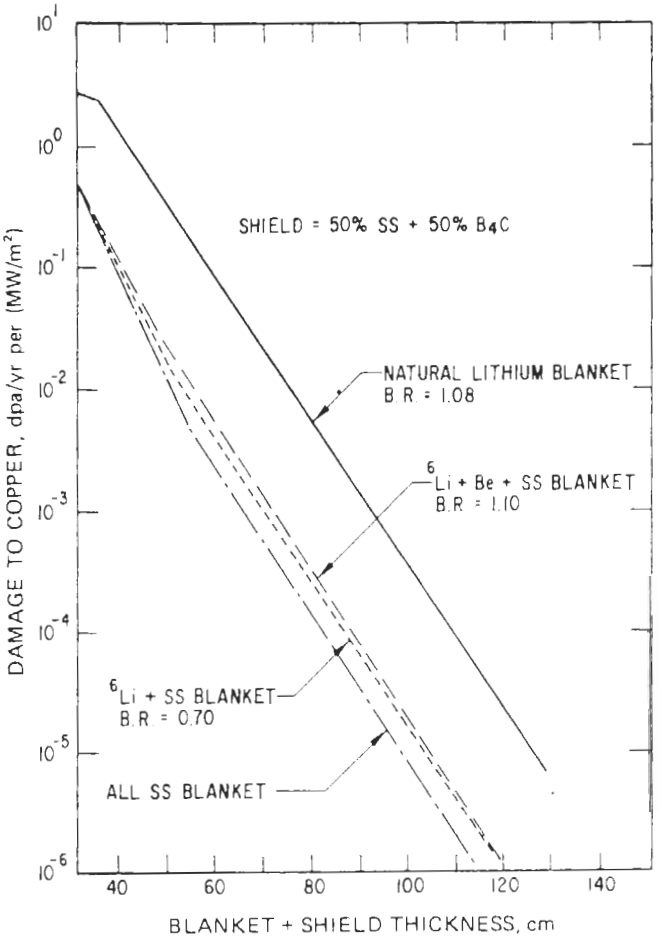

Fig. 19. Displacement damage to superconductor stabilizer (copper) versus overall blanket/shield thickness for selected tritium-breeding blanket-materials configurations.

VIII.C. Mechanical Design Considerations

VIII.C.1. Remote Maintenance and Repair

All aspects of maintenance, repair, or modification necessarily will be done with remote handling equipment due to the residual radioactivity from fusion neutrons. Thus all components of the PECS and the reactor need to be designed for remote handling, a very impressive task considering the size, weight, and geometric complexities encountered.

The proposed TEPR design has provisions for assembly and disassembly of the blanket and shield in separate or separately joined pairs of block sections (see Fig. 20). The blanket and shield pieces are removed from between the TF coils using an overhead crane for the top members and special lift vehicles for the lower units. Remote removal of the vacuum apparatus is done in the same manner with all components and subcomponents designed specifically for remote coupling. All coolant connections will also be done with remotely operated equipment.

Maintenance, repair, and inspection of the vacuum wall will be done with specially designed machines that will be inserted into the torus through either the vacuum ports or the experimental access ports. A full-size section of the PECS will be maintained as a mockup housing duplicate servomachines. Using the mockup and servomachines in planographic coupling with the reactor units, pretested repairs or assembly activities may be duplicated within the reactor with technicians guiding the manipulation utilizing television cameras.

VIII.C.2. First-Wall Vacuum Chamber

The first wall is an independently supported structure that will be cooled using a separate circuit from the blanket. Both helium and water are under consideration. Water cooling has more apparent advantages, including smaller coolant channels, simple manifolding and routing, lower temperature operation (620°F) away from the

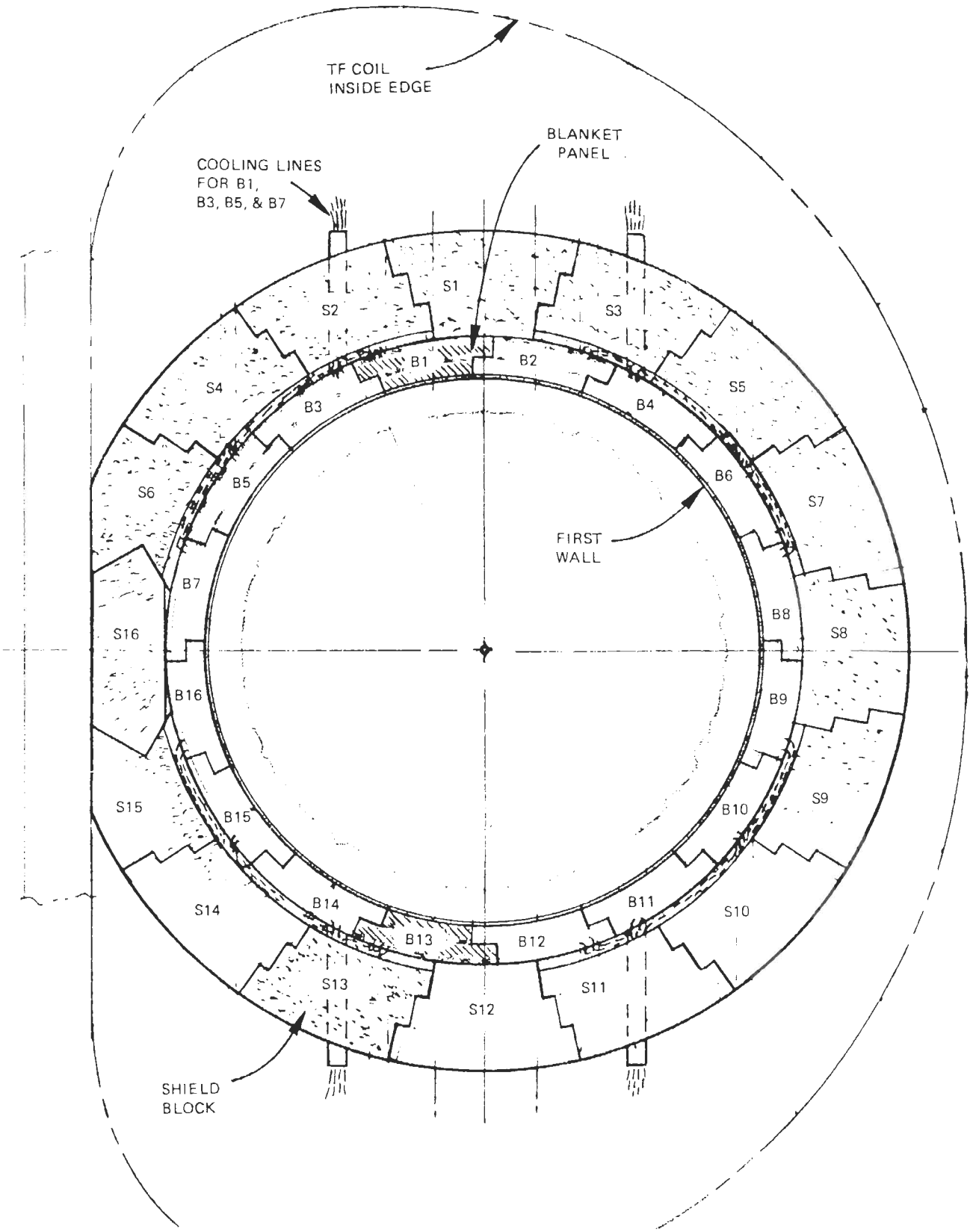

Fig. 20. Blanket/shield segmentation.

creep range, low pumping power, and ease of locating and repairing leaks. Disadvantages are thermal gradient problems associated with placement and attachment of coolant tubing, high pressure requirements to 2000 psi, tritium buildup in the water system, and radioactivity buildup in the water system.

Inner-mounted coolant panels consist of a 1-cm-thick stainless-steel plate with coolant tubes and headers affixed to the outer convex surface and coated with a low-Z material on the inner concave surface. The panels are held to the wall with constant pressure fasteners. Supply and return manifolds extend circumferentially around the chamber in pockets at the junction of the vessel segments.

VIII.C.3. Blanket

The present blanket design effort for the TEPR segments the blanket annulus into contoured blocks, 16 blocks make up an annular wedge section, and a total of 32 wedge sections make up the complete blanket, 512 pieces in all. Each of these contoured blocks is an average of 1 m in length, weighs ~2 tons, and contains coolant piping and lead connections, standoff insulation, and support to the companion shield, torque limiters, and handling fittings. Cooling systems designs using all helium and all water are being carried.

VIII.C 4. Shield

The geometrical arrangement of the shield is similar to that of the blanket (Fig. 20). There are 512 pieces of shielding, the largest ~13 tons, the smallest ~2 tons. The major shield design problems are found in trying to minimize fabrication costs of this large volume of materials.

IX. TRITIUM PROCESSING AND CONTAINMENT

Operation at a cycle-averaged power of ~100 MW(th) will result in the consumption (by burnup) of ~16 g/day of tritium and ~11 g/day of deuterium. Taking into account the fractional burnup and the extent to which a cold-fuel gas blanket is employed, the gross fuel throughput could approach 2700 g/day (D + T). The cost of supplying tritium to the TEPR to offset the burnup may run from 5 to 15 million $/yr, for a 30% plant duty factor. The fueling costs associated with deuterium supply are negligible.

The tritium-handling facility for Stage I operation has been broken down into six major systems: fuel delivery, fuel circulation, fuel processing, fuel storage, in-plant containment, and purge processing. Stage II operation requires all six of these systems plus an additional system to provide blanket processing. The principal features of these systems, as they are currently conceived, are outlined below. A schematic drawing of the mainstream fuel cycle is shown in Fig. 21.

IX.A. Fuel Delivery System

The function of this system is vital to sustained operation of reactor level plasmas in a TEPR. A substantial fraction of the total quantity of D-T fuel involved in a single burn cycle may have to be delivered to the plasma after initiation of the discharge. Fueling schemes that involve either high-speed injection of solid D-T pellets or application of a cold D-T gas blanket are leading candidates.

IX.B. Fuel Circulation System

The tritium handling facility for the TEPR is comprised of a network of systems that either operate on or store the fuel at various stages of the fuel cycle. The subsystems and components that fall under the fuel circulation system are those that provide the interfaces between the other six tritium handling systems, e.g., all interconnecting ductwork and piping, compressors, circulation pumps, vacuum pumping equipment, numerous intermediate conditioning steps, monitoring equipment, overall facility-control center, valves, by-passes, etc.

IX.C. Fuel Processing System

This system consists of an integrated process involving a hot-getter/cryogenic-trap step (to remove nonhydrogenous impurities) and a cryogenic-distillation step (to remove helium and protium). Alternatives to cryogenic distillation, including laser-excited isotope separation and multistaged permeable membranes, will eventually come under study.

IX.D. Fuel Storage System

Various approaches to the provision of fail-safe fuel storage and storage access are being investigated. For the purposes of the present design study, consideration is given to a concrete-barricaded vault containing three or more independently controlled storage cells. The cells house a temperature-sensitive hydrogen-gettering material, wherein uptake or release is controlled by temperature adjustments. The vault itself is provided with a quenching system that can rapidly remove thermal energy from the cells in the event of an incident that could compromise the storage of tritium. Also included in the assessment of this

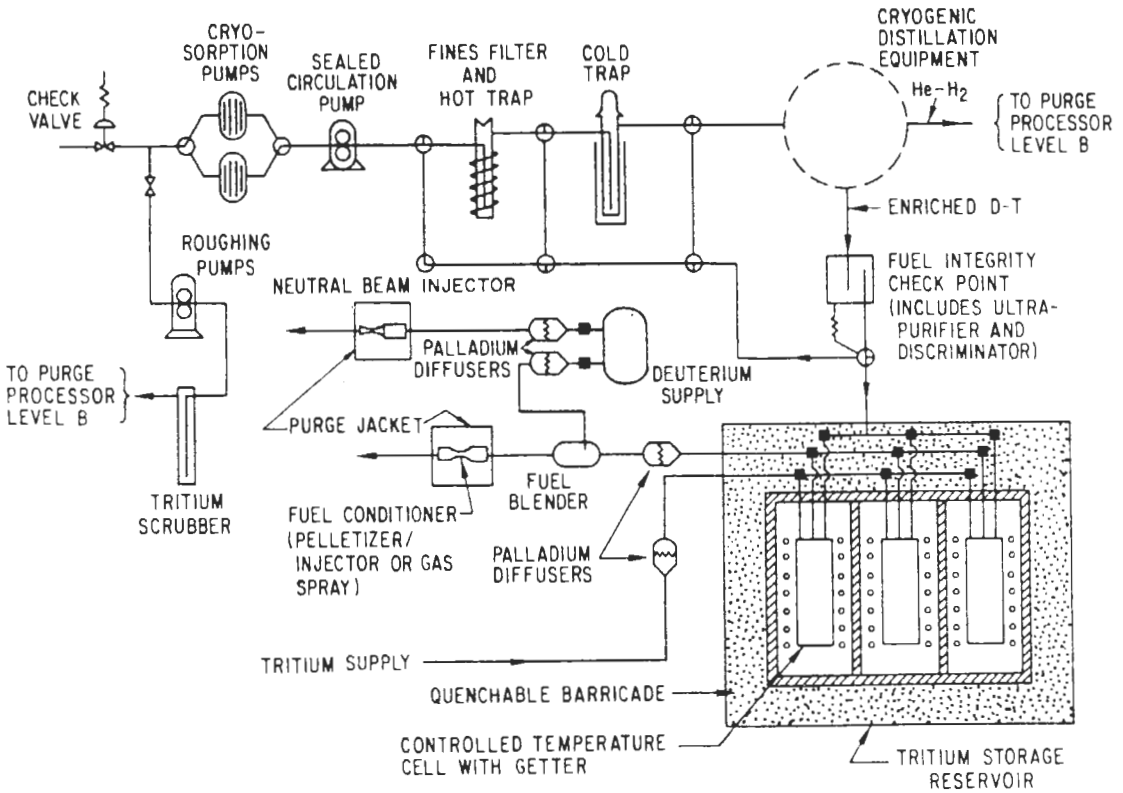

Fig. 21. Preliminary fuel-cycle schematic for the TEPR.

system are those considerations that are pertinent to fail-safe transportation of tritium from a distant production facility. Prospects for near-term development of the required transportation and storage facilities based on existing technology appear to be excellent.

IX.E. In-Plant Containment System

Current thinking on this system suggests that consideration be given to three levels of tritium containment. Where it is possible to do so, construction of all components that come into direct contact with tritium should be made with low-permeability materials (e.g., selected alloys, metal composites, ceramic barriers), particularly in elevated temperature ($>300°C$) regions. It may be necessary to provide an external, closely-fitted jacket with provision for in-jacket purging around those tritium facility components that:

1. are susceptible to failure
2. operate at elevated temperature
3. contain relatively large quantities of tritium.

In addition, the main reactor hall and the other in-plant rooms that house tritium-handling systems will be designed to include hermetic sealing (from the environment) and an inert continuously processed atmosphere.

IX.F. Purge Processing System

This system must be designed to remove tritium from both the jacketed and whole-room purge streams. Besides removing tritium from these purge streams under normal operating conditions, it will have to be capable of:

1. handling all plausible forms of high-level tritium release
2. providing sufficient enrichment of tritium in protium-contaminated, purge-stream effluents to permit its return to the mainstream fuel cycle.

IX.G. Blanket Processing System

This system is essential to Stage II operation. During recent years, considerable attention has been given to tritium recovery from various potential blanket materials. Two promising methods for removing tritium from liquid-lithium blankets are being given serious consideration at this time. One involves the removal of tritium (as LiT) and other salt-like impurities (e.g., Li_3N,

Li_2C_2, and Li_2O) from the lithium blanket by extraction with an appropriately selected molten salt. The second consists of extraction of tritium from liquid lithium in a fluidized bed of a finely divided, solid, hydrogen-gettering material.

X. RESEARCH AND DEVELOPMENT REQUIREMENTS

The TEPR preliminary conceptual design described in this paper represents a significant extrapolation of several technologies, even though an effort was made to minimize such extrapolations to the extent that this was consistent with the TEPR objectives. Identification of research and development requirements for the TEPR was an integral part of this study. The principal research and development requirements are summarized in this section.

X.A. Blanket and Shield Technology

Improved nuclear data and radiation transport computational methods must be developed and verified with integral experiments. Primary coolant technology (coolant chemistry, heat transfer and pressure drop data, compatibility, thermal-fluid computational methodology, components, etc.) must be improved for the Stage I coolant (H_2O or helium) and must be developed for lithium for Stage II. Structural analysis computational methodology must be extended. Experimental confirmation of first-wall cooling and structural integrity must accompany the design effort. Methods for the measurement of impurity concentrations in the blanket and coolant must be developed.

X.B. Superconducting Magnets

Basic data relevant to a better understanding of cryogenic stability of superconducting magnets are required. Analytical and experimental work on coil and conductor stability and on ac losses must be carried out. Conductor and cable development is needed for both steady-state (TF coil) and pulsed (OH and EF coil) magnets. Questions regarding mechanical stresses, coil interactions, handling, winding, etc. must be resolved. Magnet technology should be demonstrated on prototypes in those cases where a small-scale modeling is appropriate.

X.C. Materials

One major set of materials problems is associated with the first wall. Low-Z coating technology must be established and the effects of the chemical, thermal, and radiation environment of the first wall on the coating must be understood. Data on first-wall erosion rates due to sputtering, blistering, etc. must be developed for bare and coated stainless steel. Irradiation effects on the mechanical properties of austenitic stainless steel must be understood. Chemical, thermal, and irradiation effects on electrical insulators, which can be used as flux breakers, must be determined. Outgassing data must be developed. The technology for advanced structural materials (e.g., vanadium alloys) for Stage II must be developed.

A second major set of materials problems is associated with the TF coil. The irradiation effects on superconductor, stabilizer, insulator, and structural materials at 3 to 4.2 K must be understood. Data on the thermal, electrical, and mechanical properties of structural materials at 3 to 4.2 K must be developed.

X.D. Plasma Heating and Fueling

Energy recovery technology and/or negative ion sources must be developed for the neutral-beam injector systems. Radio-frequency heating technology should be developed as a backup method. Technology must be developed for the initial breakdown of the plasma and for refueling the plasma during operation.

X.E. Plasma Physics

Confinement, impurity control, heating, refueling, MHD stability limitations, and configurational stability of noncircular cross-section plasmas are foremost among the plasma physics uncertainties that must be better understood.

X.F. Tritium Handling

Isotope separation technology, materials for tritium containment, and tritium control technology must be developed for Stage I of the TEPR. The technology for recovering tritium from lithium blankets must be developed for Stage II.

X.G. Vacuum Systems

Large cryosorption panels must be developed for the neutral beam injection system, and large cryosorption pumps must be developed for the toroidal vacuum system. Lead-tight canned mechanical pumps must be developed for the roughing system.

X.H. Remote Maintenance, Assembly, and Fabrication

Special devices must be developed to perform the remote maintenance and assembly/disassembly operations that will be required for the TEPR. Component fabrication also requires development.

X.I. Energy Storage and Switching

An energy storage system that is matched to the requirements of the OH system must be developed. Energy switching technology must be developed for the neutral injection system.

ACKNOWLEDGMENT

This work was performed under the auspices of the U.S. Energy Research and Development Administration.

REFERENCES

1. S. O. DEAN et al., "Fusion Power by Magnetic Confinement," WASH-1290, U.S. Atomic Energy Commission (1974); see also, "Tokamak Fusion Reactor Research and Development Plan," U.S. Energy Research and Development Administration/Division of Controlled Thermonuclear Research (1975).

2. W. M. STACEY, Jr. et al., "Tokamak Experimental Power Reactor Studies," ANL/CTR-75-2, Argonne National Laboratory (1975).

3. "Two Component Torus–Joint Conceptual Design Study," Princeton Plasma Physics Laboratory and Westinghouse Electric Corporation (1974).

4. S. O. DEAN et al., "Status and Objectives of Tokamak Systems for Fusion Research," WASH-1295, USAEC/DCTR, U.S. Energy Research and Development Administration/Division of Controlled Thermonuclear Research (1974).

5. "Decharges a Fort Courant dans TFR," *Proc. Conf. Plasma Physics and Controlled Nuclear Fusion Research*, Paper A6-2, Tokyo (1974).

6. R. G. MILLS, Ed., "A Fusion Power Plant," MATT-1050, Princeton Plasma Physics Laboratory (1974).

7. G. L. KULCINSKI et al., "UWMAK-I–A Wisconsin Toroidal Fusion Reactor Design," UWFDM-68, University of Wisconsin (1973).

8. B. B. KADOMTSEV and P. P. POGUTSE, "Trapped Particles in Toroidal Magnetic Systems," *Nucl. Fusion*, **11**, 67 (1971).

9. F. W. WIFFEN and E. E. BLOOM, "Effect of High Helium Content on Stainless-Steel Swelling," *Nucl. Technol.*, **25**, 113 (1975).

10. *Irradiation Embrittlement and Creep in Fuel Cladding and Core Components*, British Nuclear Energy Society, London (1972).

11. T. T. CLAUDSON, "Materials Considerations in Support of the FFTF Preliminary Safety Analysis," HEDL-TME-71-53, Hanford Engineering Development Laboratory (1971).

12. P. SOO and J. McANDREW, "Type 304 and 316 Stainless Steel Data for High Temperature Design," WARD-3045T2C-3, Westinghouse Advanced Reactors Division (1972).

13. J. FILE, R. G. MILLS, and G. V. SHEFFIELD, "Large Superconducting Magnet Design for Fusion Reactors," *IEEE Trans. Nucl. Sci.*, **NS-18**, 277 (1974).

14. J. M. GREENE, J. L. JOHNSON, and C. E. WEIMER, "Tokamak Equilibrium," *Phys. Fluids*, **14**, 671 (1971).

15. K. W. EHLERS et al., "Large-Area Plasma Sources," *Proc. 2nd Symp. Ion Sources and Formation of Ion Beams*, Oct. 22-25, 1974, Berkeley, California, LBL-3399, paper I-5 (1974).

16. R. C. DAVIS et al., "A Multi Ampere DuoPIGatron Ion Source," *Rev. Sci. Instrum.*, **43**, 278 (1972).

17. G. NEWSTEAD, "The Homopolar Generator," *Sci. J.*, **3**, 55 (1967).

18. P. F. SMITH and J. D. LEWIN, "Superconducting Energy Transfer Systems," *Particle Accelerators*, **1**, 155 (1972).